Molecular Force and Velocity Measurements During the Latch-State

Megan Hammell

Department of Biomedical Engineering
McGill University, Montreal

December 2021

A thesis submitted to McGill University in partial fulfillment of the requirements of the degree of Master of Engineering

Abstract

Smooth muscle has the unique ability to maintain force for long periods of time at low energy cost. This characteristic is called the latch-state and occurs more frequently in tonic than phasic smooth muscle. Although many theories have been proposed to explain the latch-state, all were based on tissue level measurements and have yet to be verified at the molecular level. One such theory suggests that, if myosin is dephosphorylated while attached to actin, it will remain attached and maintain force. To elucidate the underlying mechanism of the latch-state, myosin light chain phosphatase (MLCP) was injected in the laser trap assay while measuring the force generated by a population of tonic or phasic smooth muscle myosin (SMM) molecules pulling on a single actin filament. To further understand the effect of dephosphorylation on the SMM molecular mechanics, MLCP was also injected during *in vitro* motility assays consisting of 100% tonic or phasic SMM and *in vitro* motility mixture assays consisting of 25% skeletal muscle myosin (SKM) and 75% tonic or phasic SMM, while measuring the velocity (v) and fraction of moving actin filaments (f_{mot}). The *in vitro* motility assays provided information regarding the time course of SMM deactivation, whereas the rationale behind the mixture assays was that, since SKM is not regulated by phosphorylation, a transient decrease in v and/or f_{mot} due to the load imposed by attached, dephosphorylated SMM (latch-bridges) should be observed if the latch-state occurs. Additionally, v and/or f_{mot} should eventually increase to the level of SKM following latch-bridge detachment. Flow-through chambers with a top opening covered by a microporous membrane to allow diffusion of MLCP without creating bulk flow were optimized and improved the quality of molecular mechanics measurements. Force maintenance post MLCP injection was statistically longer for tonic than phasic SMM. The rate at which f_{mot} decreased during the *in vitro* motility assays was not statistically different between tonic and phasic SMM, but the rate at which v decreased was statistically less for tonic than phasic SMM. A transient decrease was not observed in v or f_{mot} during the *in vitro* motility mixture assays for either the tonic-skeletal or phasic-skeletal mixtures. The steady-state magnitude of v post MLCP injection (v_2) was not statistically different between the tonic-skeletal and phasic-skeletal mixtures, but the time required to reach v_2 post MLCP injection (t_2) was statistically greater for the tonic-skeletal mixture. Taken together, these data do not suggest the presence of a load during dephosphorylation and as such, do not support the theory of latch-bridge formation. Instead, these data suggest that dephosphorylation has a different effect on tonic and phasic SMM; specifically, dephosphorylated tonic SMM may continue cycling longer

than dephosphorylated phasic SMM, which could contribute to the greater propensity of tonic muscle to enter the latch-state.

Résumé

Le muscle lisse a la capacité unique de maintenir la force pendant de longues périodes à faible coût énergétique. Cette caractéristique est appelée l'état “latch” et se produit plus fréquemment dans le muscle lisse tonique que phasique. Bien que de nombreuses théories aient été proposées pour expliquer l'état latch, toutes étaient basées sur des mesures au niveau des tissus et doivent encore être vérifiées au niveau moléculaire. Une de ces théories suggère que, si la myosine est déphosphorylée alors qu'elle est attachée à l'actine, elle restera attachée et maintiendra la force. Pour élucider le mécanisme sous-jacent de l'état latch, la phosphatase de chaîne légère de myosine (MLCP) a été injectée pendant des mesures, faites à l'aide de pinces optiques, de la force générée par une population de molécules de myosine des muscles lisses (SMM) tonique ou phasique, sur un seul filament d'actine. Pour mieux comprendre l'effet de la déphosphorylation sur la mécanique moléculaire de la SMM, la MLCP a également été injectée lors d'essais de motilité *in vitro* constitués de SMM 100% tonique ou phasique, ainsi que d'essais de motilité *in vitro* constitués de mélange de 25% de myosine du muscle squelettique (SKM) et 75% de tonique ou SMM phasique, tout en mesurant la vitesse (v) et la fraction des filaments d'actine en mouvement (f_{mot}). Le test de motilité *in vitro* a fourni des informations concernant l’évolution dans le temps de la désactivation du SMM, tandis que le test du mélange SMM-SKM a permis de vérifier, étant donné que la SKM n’est pas régulée par la phosphorylation, si une diminution transitoire de v et/ou de f_{mot} était observée en raison d’une charge imposée par la SMM attachée et déphosphorylée (ponts latch). De plus, v et/ou f_{mot} devraient éventuellement augmenter jusqu'au niveau de SKM après le détachement des ponts latch. Les chambres à circulation avec ouverture supérieure recouverte d'une membrane microporeuse pour permettre la diffusion de MLCP sans créer d'écoulement en vrac ont été optimisées et ont amélioré la qualité des mesures de mécanique moléculaire. Le maintien de la force après l'injection de MLCP était statistiquement plus long pour le SMM tonique que phasique. La diminution de f_{mot} au cours des tests de motilité *in vitro* n'était pas statistiquement différente entre la SMM tonique et phasique, mais la diminution de v était statistiquement moindre pour la SMM tonique que phasique. Une diminution transitoire n'a pas été observée dans v ou f_{mot} pendant les essais de motilité *in vitro* pour les mélanges tonique-squelettique ou phasique-squelettique. L'état d'équilibre de v après l'injection de MLCP (v_2) n'était pas statistiquement différente entre les mélanges tonique-squelettique et phasique-squelettique, mais le temps nécessaire pour atteindre v_2 après l'injection de MLCP (t_2) était statistiquement plus grand pour le

mélange tonique-squelettique. Prises ensemble, ces données ne suggèrent pas la présence d'une charge pendant la déphosphorylation et donc, ne soutiennent pas la théorie de la formation de pont latch. Au lieu de cela, ces données suggèrent que la déphosphorylation a un effet différent sur la SMM tonique et phasique. Plus précisément, le SMM tonique déphosphorylée peut continuer à cycler plus longtemps que le SMM phasique déphosphorylée, ce qui pourrait donner une plus grande opportunité au muscle tonique d'entrer dans l'état latch.

Acknowledgements

First and foremost, I would like to thank Dr. Anne-Marie Lauzon for her exceptional mentorship and supervision over the past three years. Her endless support and encouragement greatly contributed to making my graduate school experience enjoyable, and I am forever grateful for everything that I learned under her guidance.

I would also like to thank all past and present members of the Lauzon Lab for helping create such a fun and supportive atmosphere that never failed to bring a smile to my face. In particular, I would like to thank Dr. Gijs IJpma for his indispensable advice and insight into this project, as well as for always having a new idea at the ready when I felt like I had hit a roadblock. I would also like to thank Linda Kachmar for her invaluable help in preparing the stock materials required for my experiments, Zsombor Balassy for the time he spent training me when I first joined the lab, and Genevieve Bates for helping me improve my nitrocellulose-coating skills.

I thank Mr. Michael Alveis from Marvid Poultry for the procurement of the chicken gizzards and acknowledge the financial support of the Natural Sciences and Engineering Research Council of Canada (NSERC). Lastly, I am honoured to be a recipient of the Excellence Award from the Department of Biomedical Engineering.

Contribution of Authors

Megan Hammell and Dr. Anne-Marie Lauzon conceptualized the objectives of this thesis and designed the experiments. Megan Hammell performed the experiments, analyzed the data, prepared all the graphs, charts and illustrations, and wrote the entire thesis. Linda Kachmar purified the myosin from chicken gizzard and pectoralis, and prepared the following: the actin, the gelsolin-coated microspheres, and the stock buffers for the laser trap and *in vitro* motility assays. Nedjma Zitouni contributed to the chicken gizzard myosin purification as well. Dr. Gijs IJpma developed the software used to measure the microsphere displacement in the laser trap assay, as well as the software used to measure the actomyosin mechanics in the *in vitro* motility assays. Dr. Gijs IJpma also contributed to the optimization of both the laser trap stiffness calibration protocol and the equipment used to perform injections during the laser trap and *in vitro* motility assays. Zsombor Balassy conceived the rationale of using the *in vitro* motility mixture assay to test for a load and developed the first version of the flow-through chamber and injection protocol used in this thesis. Zsombor Balassy also developed the software used to record videos during the *in vitro* motility assays, and the model used to fit the *in vitro* motility assay data. Megan Hammell, Dr. Anne-Marie Lauzon and Dr. Gijs IJpma contributed to the interpretation of the results of this thesis. Dr. Anne-Marie Lauzon edited the draft of this thesis.

Table of Contents

List of Figures

List of Tables

List of Abbreviations

ADP	Adenosine diphosphate
ATP	Adenosine triphosphate
ATPγS	Adenosine gamma-thio triphosphate
BSA	Bovine serum albumin
Ca^{2+}	Calcium
CCD	Charge-coupled device
ERK	Extracellular signal-regulated kinase
F	Force exerted by myosin on the actin-microsphere system in the laser trap assay
F-actin	Filamentous actin
F_f	Viscous drag (Stokes) force
f_{mot}	The percentage of actin filaments moving faster than a given cut-off velocity (motile fraction) in the *in vitro* motility assay
m_{fmot}	The rate of change in f_{mot} during the second phase of the piecewise model fit
G-actin	Globular actin
HMM	Heavy meromyosin
HSC	High salt conditions
(+)insert	Inserted smooth muscle myosin heavy chain isoform
(-)insert	Non-inserted smooth muscle myosin heavy chain isoform
k	Laser trap stiffness
k_c	Laser trap stiffness interpolation constant
LC_{20}	Myosin regulatory light chain
L_f	Average length of stopped and moving actin filaments in the *in vitro* motility assay
LP	Laser power
LSC	Low salt conditions
MgADP	Magnesium adenosine diphosphate
MgATP	Magnesium-adenosine triphosphate
MgATPγS	Magnesium-adenosine gamma-thio triphosphate

MLCK	Myosin light chain kinase
MLCP	Myosin light chain phosphatase
NEM	N-ethylmaleimide myosin
η	Dynamic viscosity
PETG	Polyethylene terephthalate glycol
P_i	Inorganic phosphate
PKC	Protein kinase C
r	Microsphere radius
S1	Myosin subfragment-1
SD	Standard deviation
SKM	Skeletal muscle myosin
SMM	Smooth muscle myosin
SMMHC	Smooth muscle myosin heavy chain
t	Time
t_1	Time at which the second phase of the piecewise model fit starts
t_2	Time at which the second phase of the piecewise model fit ends
T_{Hold}	Time during which force was maintained post-injection in the laser trap assay
T_{Inj}	Time of injection following the start of force generation in the laser trap assay
TRITC	Tetramethyl rhodamine isothiocyanate
v	Average velocity of all actin filaments moving faster than given cut-off velocity in the *in vitro* motility assay
m_v	The rate of change in v during the second phase of the piecewise model fit
v_c	Constant velocity
Δx	Distance that the microsphere is pulled away from the center of the laser trap
y_1	Value of f_{mot} or v during the first phase of the piecewise model fit (represented by f_{mot1} and v_1 respectively)
y_2	Value of f_{mot} or v during the third phase of the piecewise model fit (represented by f_{mot2} and v_2 respectively)

1 Introduction

1.1 Muscle Physiology

The three main types of muscle in the human body are cardiac, skeletal, and smooth [1-3]. Cardiac muscle is the heart muscle and contracts to pump blood through the circulatory system. Skeletal muscle attaches to bone and is responsible for supporting and moving the skeleton. Smooth muscle is found in the walls of hollow organs and in the blood vessels and is responsible for many different tasks, such as pushing chyme through the intestines, controlling air flow in the lungs and maintaining blood pressure. While both smooth and cardiac muscle perform involuntary contractions, skeletal muscle is under voluntary control. Although many structural and regulatory differences exist between these muscle types due to their distinct functions, the fundamental mechanism by which they each generate force and motion is similar.

1.2 Skeletal Muscle

Skeletal muscle cells (see [4] for a review) are multinucleated, cylindrically shaped, and highly organized in parallel bundles called fascicles, which in turn are surrounded by connective tissues called the endomysium, perimysium, and epimysium (Figure 1.1). They are composed of cylindrical structures called myofibrils, which lie parallel to the cell itself and contain sarcomeres connected in series (Figure 1.1). The sarcomere is considered the smallest, functional unit of skeletal muscle and is defined by the region between two consecutive cytoskeletal structures called Z-lines (Figure 1.2). Each sarcomere consists of two I bands and an A band. The I bands contain thin filaments, which are anchored to the Z-lines and primarily composed of the contractile protein actin (see section 1.4.2). The A band contains thick filaments, which are mainly composed of the contractile protein myosin (see section 1.4.1) and are anchored to the sarcomere center (M-line). The A band is comparatively darker in appearance to the I bands because of the presence of the thick filaments. The distinct pattern of alternating light and dark bands can be observed under a microscope and is the reason both cardiac and skeletal muscle are referred to as striated muscle.

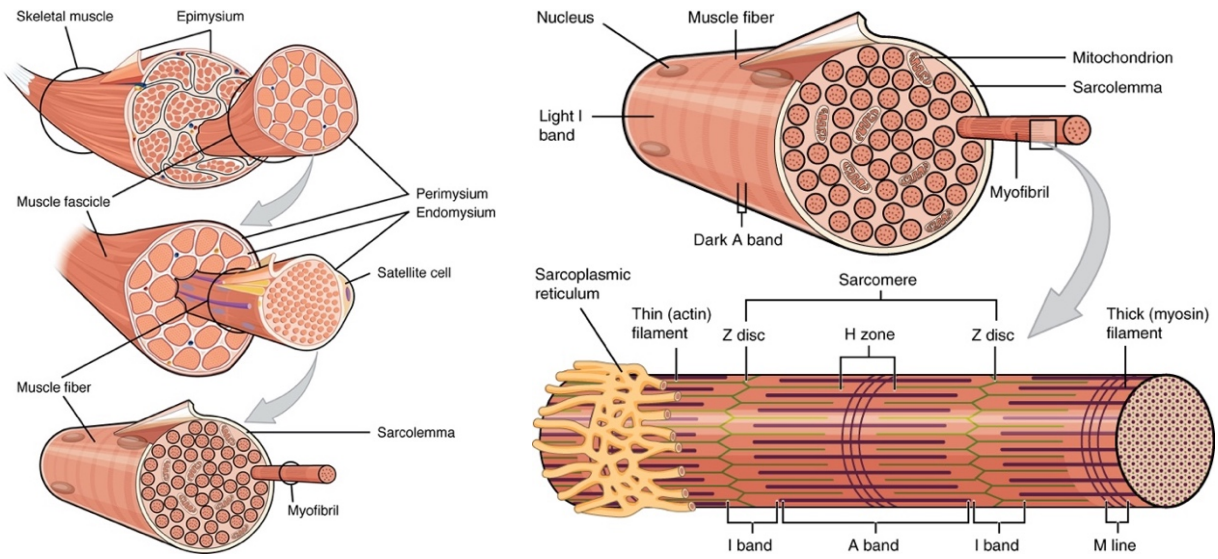

Figure 1.1: The hierarchical structure of skeletal muscle. Reproduced with permission under a Creative Commons Attribution 4.0 International license from [5]. Download for free at https://openstax.org/details/books/anatomy-and-physiology.

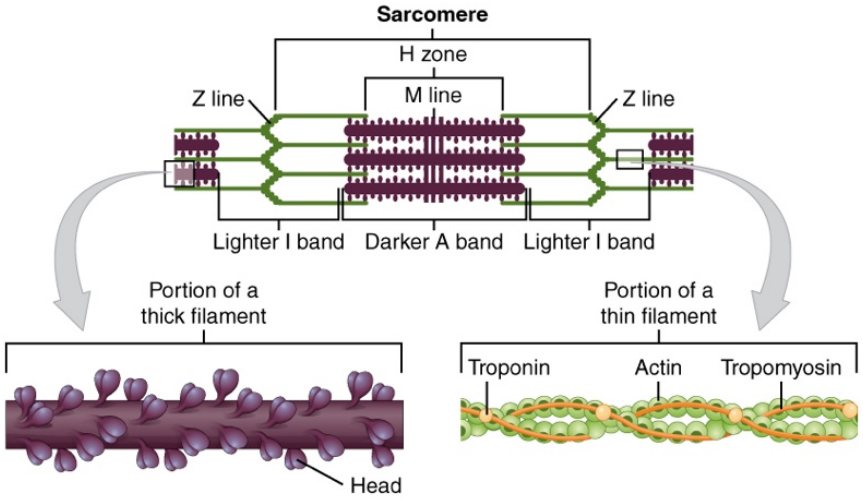

Figure 1.2: The molecular structure of a skeletal muscle sarcomere. Reproduced with permission under a Creative Commons Attribution 4.0 International license from [5]. Download for free at https://openstax.org/details/books/ anatomy-and-physiology.

The thick and thin filaments overlap within a portion of the A band such that myosin can interact with actin. Upon hydrolysis of adenosine triphosphate (ATP), myosin will bind to and pull actin such that the thin filaments slide along the thick filaments; this causes the sarcomeres to shorten

and produce a muscular contraction. In striated muscle, contraction is initiated by calcium (Ca^{2+}) [6] and regulated at the thin filament level [7] by the actin-binding proteins troponin and tropomyosin (see section 1.4.2). Tropomyosin wraps around actin such that the myosin-binding sites are blocked, and its position is regulated by troponin (Figure 1.2). When signalled by a motor neuron, Ca^{2+} enters the sarcoplasm (muscle cell cytoplasm), binds to troponin, and triggers a conformational change that moves tropomyosin out of its blocking position, allowing myosin to bind to actin.

1.3 The Cross-Bridge Cycle

The mechanism wherein thick and thin filaments slide past each other, while maintaining their respective lengths, to induce sarcomeric shortening and produce a muscular contraction is known as the sliding filament theory [8-10]. However, the specific interactions between myosin and actin during this time are described by the cross-bridge cycle (see [11] for a review) (Figure 1.3), the steps of which are as follows: myosin hydrolyzes ATP to adenosine diphosphate (ADP) and inorganic phosphate (P_i); myosin binds to actin, forming a cross-bridge; myosin undergoes a conformational change (the power stroke) that generates force and actin filament movement; myosin releases ADP while remaining attached to actin; a new ATP molecule binds to myosin, causing it to detach from actin and begin the cycle again.

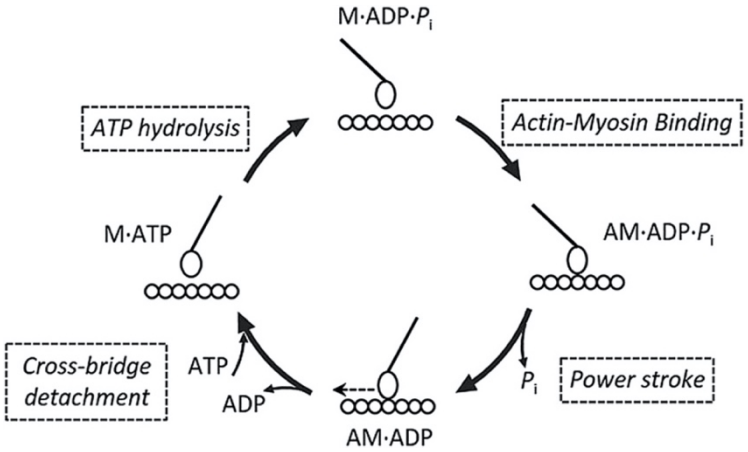

Figure 1.3: A simplified view of the cross-bridge cycle (see text for details). Reproduced with permission under a Creative Commons Attribution 4.0 International license from [12]. Download for free at https://jmg.bmj.com/ content/53/10/651.

1.4 Smooth Muscle

Smooth muscle cells (see [13] for a review) are single-nucleated, spindle-shaped and organized in sheet-like layers rather than concentric cylinders (Figure 1.4). They lack the highly organized, sarcomeric structure of skeletal and cardiac muscle cells, which explains the characteristic "smooth" rather than striated appearance of this type of muscle. Despite these differences, the molecular mechanisms used to explain contraction in striated muscle, namely the cross-bridge cycle and sliding filament theory, can also be applied to smooth muscle because their cells contain interacting thick and thin filaments. However, troponin is not present in smooth muscle cells and as such, the mechanism by which contraction is regulated is different (see sections 1.4.1 and 1.4.2). Additionally, the thin filaments are believed to be anchored to dense bodies, which are biochemically analogous to the Z-lines in striated muscle. However, this view was recently challenged by electron microscopy images that suggest dense bodies are not these focal points, but rather tubular structures aligned in parallel with the thick and thin filaments [14].

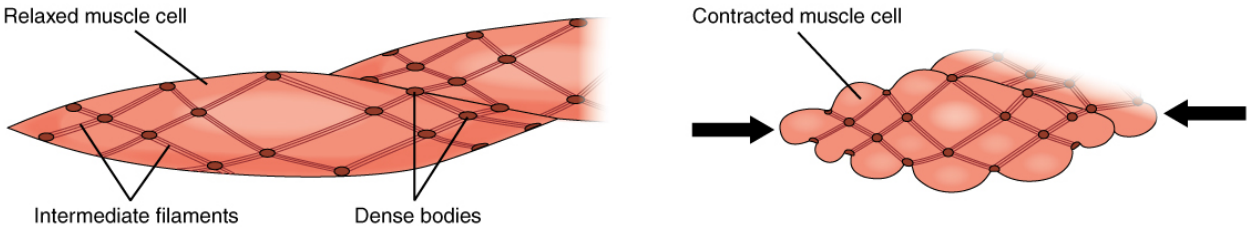

Figure 1.4: Smooth muscle cell structure while relaxed and contracted. Reproduced with permission under a Creative Commons Attribution 4.0 International license from [15]. Download for free at https://openstax.org/details/books/ anatomy-and-physiology.

There are two types of smooth muscle: phasic (single-unit) and tonic (multi-unit) muscle (see [16] for a review). Phasic muscle undergoes synchronous electrical and mechanical activity because its cells are connected by gap junctions that facilitate action potential propagation. Therefore, the primary function of phasic muscle is to propel content. For example, peristaltic waves in the digestive tract are caused by phasic muscle contractions. Conversely, tonic muscle has few (if any) gap junctions and as such, its cells act independently of each other; contraction depends both on the number of activated cells and the frequency of stimulation. These characteristics make tonic

muscle ideal for maintaining tone for long periods of time, as its name implies. For example, most blood vessels contain tonic muscle because of its effectiveness in maintaining blood pressure. Molecular differences also exist between the two smooth muscle types and are explained in detail in section 1.4.1. It should be noted that most of the time, smooth muscle cannot be categorized as purely phasic or tonic, and typically exhibit characteristics of both [17].

1.4.1 Smooth Muscle Myosin

Structure: Myosin purified from mammalian smooth muscle belongs to the class II (conventional) myosin family and is composed of two heavy chains, two regulatory light chains and two essential light chains [18, 19] (Figure 1.5). Both heavy chains contain a head (N terminus), neck, and tail (C terminus) domain. The head domain has a globular structure and contains both the ATP binding and actin binding sites. The head region is also known as the motor domain because it is where ATP hydrolysis occurs, the result of which is force generation and actin movement. The tail domains combine to form an α-helix that serves the function of filament assembly. The neck domain connects the head domain to the tail domain, binds the four light chains, and acts as a lever arm during interactions between actin and myosin [18, 20].

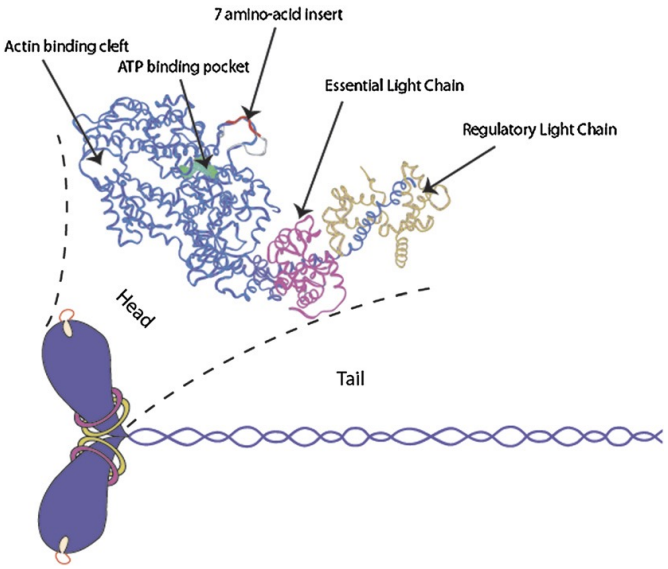

Figure 1.5: The molecular structure of a smooth muscle myosin (SMM) monomer. Reproduced with permission of the American Thoracic Society from [21]. Copyright © 2021 American

Four smooth muscle myosin heavy chain (SMMHC) isoforms can be produced by alternative splicing from a single gene [22]. Two of these isoforms differ structurally by the presence or absence of a 7-amino-acid insert (Figure 1.5) in the flexible surface loop of the head domain [23]. The inserted isoform ((+)insert) is found predominantly in phasic muscle, whereas the non-inserted ((-)insert) isoform is expressed primarily in tonic muscle [23, 24]. It has been demonstrated that, although the two isoforms generate the same unitary displacement and unitary force, the (-)insert isoform has a longer time of attachment to actin because the absence of the insert slows ADP release [25]. This characteristic explains why the (-)insert isoform propels actin filaments at half the velocity of the (+)insert isoform in the *in vitro* motility assay (see section 1.6.1) [25], as well as contributes to the higher unloaded shortening velocities observed in phasic muscle [26] [27]. There is no evidence from the literature to support a difference in force production between phasic and tonic smooth muscle so it is believed that the longer attachment time of the (-)insert isoform is accompanied by a longer total cross-bridge cycle time, thus keeping the duty cycle the same [25]. Two additional isoforms are found in the tail region of the heavy chain [28]. Although there is currently no evidence for any difference in the molecular mechanics of these two isoforms, it is believed that they contribute to mechanical differences at the tissue level because they do not assemble in the same manner [29].

Regulation: Unlike striated muscle, the mechanism by which smooth muscle contraction is regulated occurs at the thick filament level [30]. Before smooth muscle myosin (SMM) can interact with actin and initiate cross-bridge cycling, it must be activated as follows: Ca^{2+} enters the cell and binds to the protein calmodulin; the Ca^{2+}-calmodulin complex activates the enzyme myosin light chain kinase (MLCK); the Ca^{2+}-calmodulin-MLCK complex phosphorylates the myosin regulatory light chain (LC_{20}) and completes the activation process. Conversely, the myosin light chain phosphatase (MLCP) enzyme deactivates SMM by dephosphorylating the LC_{20}. Unphosphorylated myosin does not remain in the filamentous form. Moreover, unphosphorylated myosin has its heads bent down and its tail curled around the heads such that it cannot interact with actin (10S conformation). It is possible to bring back unphosphorylated myosin to the

extended conformation (6S) *in vitro* by putting it in high salt conditions. In such conditions, unphosphorylated SMM can bind to actin, but with a force that is approximately one tenth of the force generated in its phosphorylated state [31]. This is because unphosphorylated SMM does not have the ability to hydrolyze ATP [32].

It is worth noting that, although regulatory light chain phosphorylation is not necessary in skeletal muscle because its myosin-actin interactions are thin filament regulated, it remains possible [33]. Indeed, it has been demonstrated that regulatory light chain phosphorylation increases the duty cycle of skeletal muscle myosin (SKM) [34], as well as the following three characteristics in skeletal muscle tissues: ATPase rate, tension development rate, and tension magnitude [35, 36]. Essential light chain function remains unclear, but its removal has been shown to decrease the velocity of actin filaments being propelled by SKM in the *in vitro* motility assay (see section 1.6.1) [37] and to decrease force production in the microneedle assay [38]. It was suggested that this occurred due to a reduction in the strength of the myosin neck domain [39].

1.4.2 Smooth Muscle Actin and Regulatory Proteins

Actin: Actin (Figure 1.6) has both a monomeric form (G-actin) and filamentous form (F-actin), the latter of which has a double helix structure [40, 41] and binding sites for myosin, caldesmon, calponin, tropomyosin and MLCK [41-44]. Actin filaments are polarized: polymerization occurs primarily at the barbed (+) end, whereas depolymerization predominantly takes place at the pointed (-) end [45]. Furthermore, all myosin species move toward the barbed (+) end of an actin filament, except for myosin VI, an unconventional myosin that moves towards the pointed (-) end and is thought to play a role in vesicular transport [46]. Six actin isoforms exist in vertebrate muscle: α-skeletal, α-cardiac, α-vascular, β-cytoplasmic, γ-cytoplasmic and γ-enteric [42, 47]. In smooth muscle, the α-vascular and γ-enteric isoforms are associated with the contractile thin filaments and often referred to as smooth muscle actin isoforms. Comparatively, the β-cytoplasmic and γ-cytoplasmic isoforms are specific to the non-contractile cytoskeleton and commonly referred to as non-muscle isoforms [42]. Interestingly, Harris *et al*. showed that there is no difference between the velocity of actin filaments purified from smooth muscle versus skeletal muscle when being propelled by either SMM or SKM in the *in vitro* motility assay (see section 1.6.1) [48]. Indeed, the only observable difference between skeletal muscle actin and smooth muscle actin in the *in*

vitro motility assay is that the latter yields shorter filaments [41]. As such, skeletal muscle actin is often used in molecular mechanics studies because it is easier to purify and polymerize compared to smooth muscle actin.

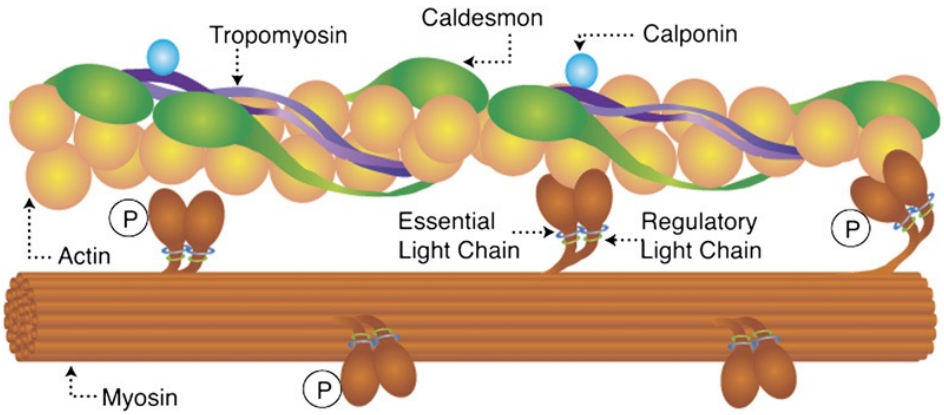

Figure 1.6: The molecular structure of smooth muscle. The thick filament (brown) is composed of myosin heavy chains and light chains (essential and regulatory), whereas the thin filament is composed of actin (yellow) and the following actin-binding proteins: tropomyosin (purple), caldesmon (green) and calponin (blue). Reproduced with permission of the American Thoracic Society from [21]. Copyright © 2021 American Thoracic Society. All rights reserved. Proceedings of the Annals of the American Thoracic Society is an official journal of the American Thoracic Society.

Tropomyosin: Tropomyosin (Figure 1.6) is a long, rod-shaped molecule that binds to actin in a coiled manner and spans the entire filament length [49]. As discussed in section 1.2, the role of tropomyosin in the regulation of striated muscle is well understood [50, 51]. Its function in smooth muscle is less clear due to the absence of troponin, but it is believed that tropomyosin increases cooperativity between cross-bridges [52].

Caldesmon: Caldesmon (Figure 1.6) is an actin-binding protein that also has myosin, tropomyosin and calmodulin binding sites [42]. It decreases actin-activated myosin ATPase activity [53], as well as actin filament velocity in the *in vitro* motility assay (see section 1.6.1) [54, 55]. Calmodulin reverses these effects, as does caldesmon phosphorylation by either extracellular signal-regulated kinases (ERK) or protein kinase C (PKC) [42, 56]. Comparatively, it has been shown that

tropomyosin accentuates the inhibitory effects of caldesmon [56-58]. Caldesmon enhances the unbinding force of unphosphorylated tonic smooth muscle myosin (from now on referred to as tonic SMM) to actin in the laser trap assay (see section 1.6.2), but reduces this force to very low levels following phosphorylation by ERK [59]. Interestingly, caldesmon is expressed in higher quantities in phasic muscle than tonic muscle [60].

Calponin: Calponin (Figure 1.6) is an actin-binding protein that inhibits actin-activated myosin ATPase activity [61, 62], as well as actin filament velocity in the *in vitro* motility assay (see section 1.6.1) [63]. The addition of Ca^{2+} and calmodulin suppresses these inhibitory effects, as does phosphorylation of calponin itself [56, 62]. It has been shown that calponin enhances the unbinding force of unphosphorylated tonic SMM to actin in the laser trap assay (see section 1.6.2), and that this effect is reversed following calponin phosphorylation [64]. Although the effects of calponin are similar to those of caldesmon, it has been demonstrated that calponin binds more effectively to actin filaments and that tropomyosin does not influence its inhibitory effect on actomyosin ATPase activity [65].

1.4.3 Comparison of Smooth and Skeletal Muscle Mechanics

Tissue level measurements showed that smooth muscle is capable of generating the same amount of force per cross-sectional area of muscle as skeletal muscle despite having one-fifth the amount of myosin [66]. However, SMM has the same unitary force and displacement as SKM [67]. Molecular mechanics studies have demonstrated a greater time of attachment to actin for SMM compared to SKM, suggesting a longer duty cycle that leads to a higher average force generation per myosin head [67]. Smooth muscle is therefore considered more efficient than skeletal muscle [68] because it consumes fewer ATP molecules due to its lower cycling rate, yet generates more force per head. Tissue level experiments have also shown that the unloaded shortening velocity of smooth muscle is one-tenth that of skeletal muscle [69]. This difference is paralleled at the molecular level, where it has been observed that SMM propels actin filaments in the *in vitro* motility assay (see section 1.6.1) at one-tenth the velocity of SKM [70]. These differences can also be explained by the comparatively shorter time period that SKM remains attached to actin during the cross-bridge cycle [67].

1.5 The Latch-State

Tonic muscle has the unique ability to maintain force for long periods of time at low energy (ATP) cost. This characteristic is known as the latch-state and was first reported by Dillon *et al*. after measuring the mechanical properties of arterial tissue during contraction [71]. Following stimulation, shortening velocity rapidly increased and reached its peak within 30 seconds, then declined to baseline within 20 minutes. LC_{20} phosphorylation level followed this trend as well. Notably, although force peaked within a similar time frame, it did not decline and was instead maintained well beyond the time at which shortening velocity and LC_{20} phosphorylation level had returned to baseline (Figure 1.7).

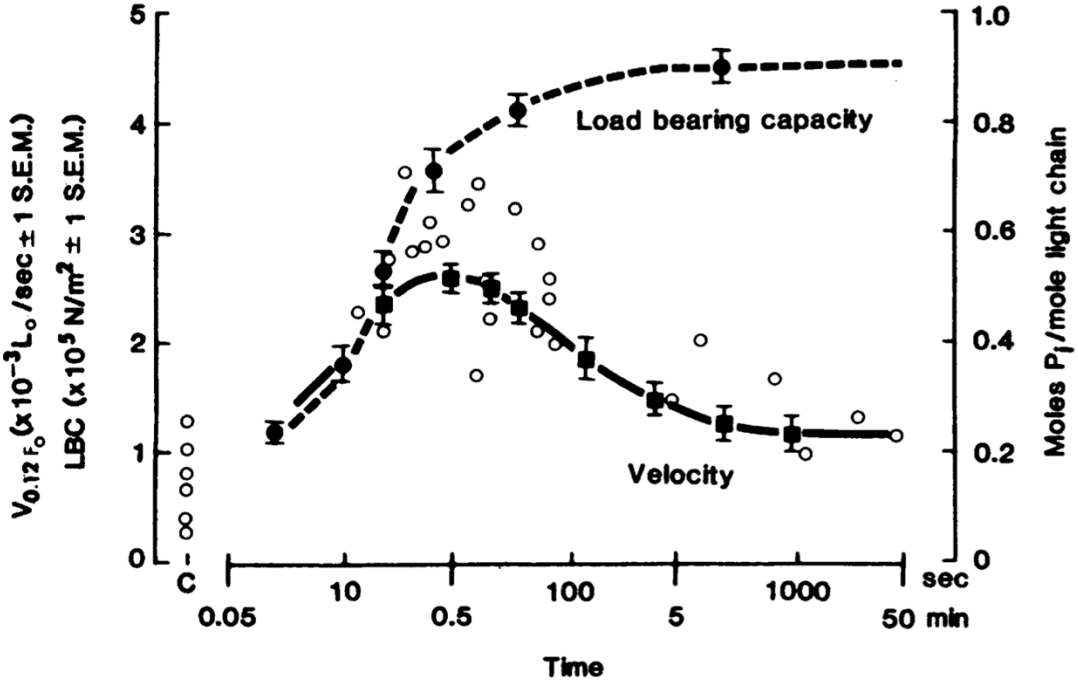

Figure 1.7: Force (dotted black line), shortening velocity (solid black line) and LC_{20} phosphorylation level (white circles) measurements following stimulation (time = 0) of arterial tissue (see text for details). Reproduced from [71] with permission from AAAS.

The underlying molecular mechanism of the latch-state has not yet been elucidated. However, many theories have been proposed to explain this economic force maintenance property. Dillon *et al*. proposed the presence of either non-cycling or slowly cycling cross-bridges (latch-bridges) that

form by LC_{20} dephosphorylation while myosin is attached to actin [71]. Since magnesium-adenosine diphosphate (MgADP) must be released from myosin before it can detach from actin, Hai and Murphy proposed that LC_{20} dephosphorylation of an attached myosin head may contribute to the development of latch simply by decreasing the rate at which MgADP is released [72, 73]. Tissue level studies further suggested that the affinity for MgADP of tonic SMM is greater than that of phasic smooth muscle myosin (from now on referred to as phasic SMM), therefore prolonging the time of attachment of tonic SMM to actin and resulting in more opportunities to enter the latch-state by LC_{20} dephosphorylation. Indeed, Fuglsang *et al*. demonstrated that the time of relaxation from rigor increased in tonic muscle, but not phasic muscle, when exposed to an increased MgADP concentration [74]. Similarly, Khromov *et al*. showed that the relaxation time of contracting tonic muscle increased following the addition of MgADP, whereas that of contracting phasic muscle was unaffected [75]. Together, these studies suggest that a greater affinity for MgADP of tonic than phasic SMM could contribute to the greater propensity of tonic muscle to enter the latch-state. Khromov *et al*. later demonstrated by measuring fluorescence transience of an MgADP analogue that the affinity of tonic muscle myosin for MgADP is increased at low phosphorylation level as well as by strain [76]. Himpens *et al.* also suggested a cooperativity mechanism to explain the latch-state, whereby the remaining phosphorylated myosin molecules facilitate the reattachment of dephosphorylated, detached myosin molecules to actin by communication via the thick filament or the actin regulatory proteins [77].

The development of molecular mechanics assays was essential for the advancement of our understanding of the molecular mechanisms underlying the latch-state. As addressed in section 1.4.1, it was shown using a laser trap assay (see section 1.6.2) that the (+) and (-)insert SMMHC isoforms exhibit a similar unitary force and displacement, but that the time of attachment to actin was twice as long for the (-)insert isoform than the (+)insert isoform [25]. The time of attachment of myosin to actin is constituted of the time for MgADP release and the time for a new magnesium-adenosine triphosphate (MgATP) molecule to enter the nucleotide binding pocket (Figure 1.3), consistent with a greater affinity of the (-)insert isoform for MgADP. Furthermore, because the (-)insert isoform is expressed predominantly in tonic muscle [23, 24], these findings are consistent with the aforementioned tissue-level results reported by Fuglsang *et al*. [74]. Other factors affecting MgADP release rate have also been explored at the molecular level. For example,

Leguillette *et al*. used an *in vitro* motility assay (see section 1.6.1) to demonstrate that the decrease in actin filament velocity caused by increasing MgADP concentration is more pronounced in tonic SMM than phasic SMM at low LC_{20} phosphorylation levels [31]. Moreover, Viegel *et al*. demonstrated using a laser trap assay that the time of attachment for a single phasic SMM monomer to actin was load-dependent; loads applied in the direction of cross-bridge movement decreased attachment time, whereas loads applied in the opposite direction increased attachment time [78].

Alternative views of the latch-state and its underlying mechanisms exist. For example, it has been suggested that non-muscle myosin is responsible for the formation of latch-bridges [79], or that single-phosphorylated SMM heads [80] contribute to the development of latch. A Ca^{2+}-dependent regulatory mechanism other than LC_{20} dephosphorylation that allows dephosphorylated myosin to reattach to actin has also been proposed [81], as well as a cooperativity mechanism between phosphorylated and dephosphorylated myosin [82, 83]. The role of actin regulatory proteins in the latch-state has also been investigated [84, 85]. Caldesmon, and calponin are of particular interest because of their known effects on actin-activated myosin MgATPase rate [53, 62], actin filament velocity in the *in vitro* motility assay [55, 56, 63] and binding force of unphosphorylated myosin [59, 64]. Furthermore, it has been speculated that caldesmon could facilitate force maintenance by acting as a cross-linker between actin and myosin [86]. Tropomyosin on the other hand may promote the latch-state by allowing cooperativity between the myosin molecules [42].

It is interesting to note that a state similar to the latch-state has also been observed in molluscan muscles; it is known as the catch-state and, like the latch-state, is characterized by high force maintenance at low energy cost [87]. Although the catch-state mechanism has not yet been elucidated, it is believed that thick filaments proteins, namely twitchin and myorod, may facilitate force maintenance by acting as cross-linkers between the thick and thin filaments [88-90].

1.6 Molecular Mechanics Measurement Techniques

1.6.1 *In Vitro* Motility Assay

The *in vitro* motility assay (Figure 1.8) is a popular method for investigating the molecular mechanics of interactions between myosin and actin. Sheetz *et al*. developed the first version of

this assay by coating fluorescent beads with SKM and observing their movement along actin filament bundles within cells from the alga, *Nitella axillaris* [91]. To address concerns regarding contamination from the *Nitella* cytoplasm, as well as the poorly defined biochemical properties of its actin bundles, Spudich *et al*. devised an updated version of the assay using only purified proteins [92]. Specifically, the *Nitella* actin bundles were replaced with arrays of oriented actin filaments reconstituted from purified muscle actin and bound to a carbon-coated electron microscope grid using severin, a protein from the amoeba *Dictyostelium*. Despite these improvements, the practicality of this assay was limited because many of the myosin-coated fluorescent beads would either remain stationary or travel only short distances, making it difficult to quantify velocity.

To overcome these issues, Yanagida *et al*. used phalloidin-rhodamine to fluorescently label F-actin and visualize individual filaments as they interacted with SKM in solution [93]. Filament movement was described as bending and characterized by both amplitude and frequency. Proteins and solutions were contained within a small gap between a glass microscope slide and glass coverslip, an apparatus now commonly referred to as a flow-through chamber. Kron *et al*. improved this assay further by immobilizing SKM filaments on the coverslip, facilitating the observation and quantification of directional actin filament movement within a single plane [94]. Toyoshima *et al*. refined this technique by using coverslips coated with nitrocellulose, and demonstrated that SKM fragments, namely heavy meromyosin (HMM) and subfragment-1 (S1), are also capable of propelling actin filaments [95].

These advancements formed the foundational elements of the *in vitro* motility assay that are still used in present-day protocols [96]: myosin (filamentous, monomeric or fragmented) is perfused in a flow-through chamber and given time to adhere to the glass coverslip; bovine serum albumin (BSA) is perfused to coat the coverslip and prevent the actin filaments from binding to it; fluorescently-labelled actin filaments are perfused and given time to bind to the myosin; buffer containing MgATP to permit cross-bridge cycling, an oxygen-scavenger to reduce photo-bleaching and methylcellulose to promote actin-myosin interactions by restricting the diffusion of the actin filaments, are in turn perfused. Small variations have emerged to improve assay practicality and the quality of molecular mechanics measurements. For example, techniques to reduce the number of non-functional myosin molecules (deadheads), which are unable to

hydrolyze MgATP and thus bind permanently to actin, have been developed to improve the quality of actin filament movement [97]. Additionally, flow-through chambers are now assembled by adhering the coverslip to the microscope slide with double-sided tape [98]; previously, grease and either plastic or glass shims were used [99]. Although nitrocellulose-coated coverslips are still commonly used, some investigators have implemented a silicon coating because of its ease of use [57, 96].

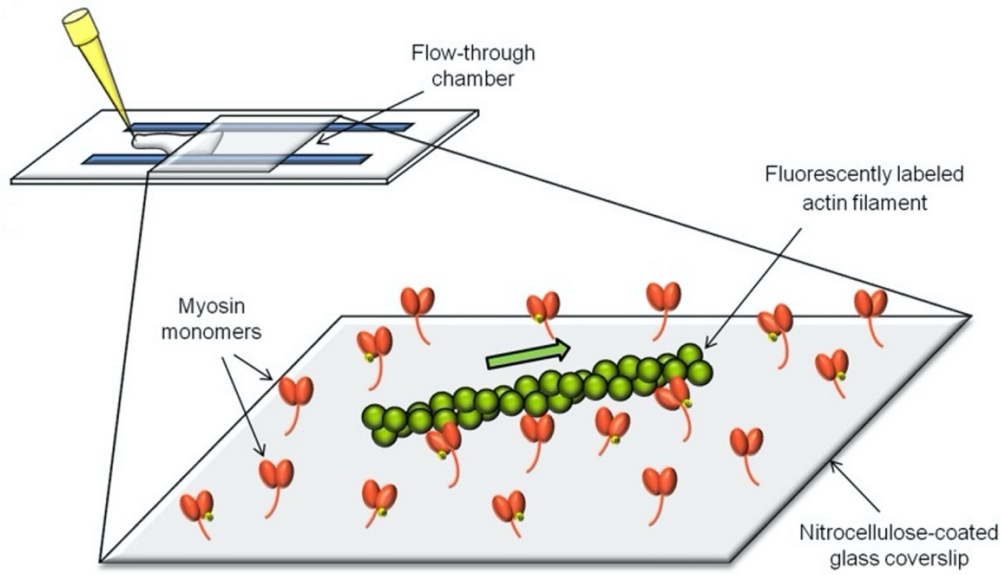

Figure 1.8: The in vitro motility assay performed with a conventional flow-through chamber. Fluorescently labeled actin filaments are propelled by myosin molecules on a glass coverslip coated with nitrocellulose (see text for details). Reproduced with permission from Genevieve Bates.

Actin filament velocity and motile fraction, the latter of which is the percentage of filaments moving faster than a threshold velocity, are two parameters that can be calculated from *in vitro* motility assays [100, 101] and have been used to evaluate the effects of physical, chemical and biological changes to the assay conditions. For example, it has been demonstrated that actin filament velocity is independent of actin filament length and dependent on MgATP concentration, ionic strength, temperature, and pH [70, 102]. It has also been shown that there is no difference in the velocity of actin filaments being propelled by either monomeric or polymeric myosin [95]. Furthermore, it has been demonstrated that actin filament velocity can be reduced by increasing

MgADP concentration or P_i concentration [103, 104], as well as by the addition of actin regulatory proteins like caldesmon and calponin [56, 57, 63]. Lastly, motility assays containing multiple types of myosin, often referred to as mixture assays, have been performed as an indirect means of investigating the relative force generation capabilities of myosin purified from different muscle types, as well as SMM that has not been phosphorylated [105, 106].

1.6.2 Laser Trap Assay

Optical trapping is a technique that uses the forces of laser radiation pressure to capture and precisely manipulate small particles, as was first reported in 1969 by Arthur Ashkin [107]. Since then, many applications of optical trapping have emerged in both the physical and biological sciences. For example, optical traps (also known as optical tweezers and laser traps) have been used in the field of atomic physics to capture and cool down atoms [108]. They have also been used with great success in the field of microbiology, largely because the wavelength emitted by an infrared laser is weakly absorbed by biological systems, and the forces exerted by the trap itself are similar to those already present in the cellular environments; these characteristics prevent the biological materials from being damaged and are the reason for which optical trapping is considered a quasi-non-invasive technique [109]. Indeed, optical traps have been used to capture and manipulate viruses, bacteria, and chromosomes [109-111], as well as estimate the material properties of organelles [112]. Moreover, the discovery of the optical trap and its application to biological systems was the reason for which Arthur Ashkin was awarded the 2018 Physics Nobel Prize [113].

Several studies that used the laser trap technique have captured microscopic beads (from now on referred to as microspheres) bound to the biological sample instead of trapping the sample itself. These microspheres are typically made from silica or polystyrene and their regular shape allows for high quality trap calibrations, which in turn increases the accuracy of the measurements [114]. The mechanism by which a microsphere is captured in an optical trap (Figure 1.9) involves the combined effects of refracted and scattered light rays [115]: the laser beam passes through a high numerical aperture microscope objective lens that refracts the light with a large angle; the refracted light rays hit the microsphere and either refract once again as they pass through, or scatter as they bounce off; the refracted light rays decelerate horizontally and accelerate downwards, causing the

microsphere to decelerate horizontally (in the opposite direction of the refracted light rays) and accelerate upwards to conserve momentum; the scattered rays counteract the accelerations caused by the refracted rays and keep the microsphere trapped in place.

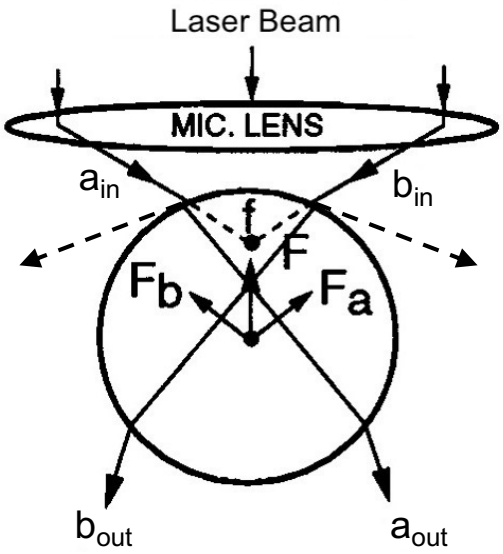

Figure 1.9: A microsphere captured in an optical trap where f is the trap focus. The refracted rays a and b give rise to the forces F_a and F_b whose vector sum F is counteracted by the force of the scattered rays (dotted lines; see text for details). Adapted with permission from [116]. Copyright (1997) National Academy of Sciences, U.S.A.

Once a microsphere is captured, the optical trap essentially functions as a linear spring; if the microsphere is pulled away from the trap center by an external force, the trap exerts an equal and opposite restorative force on the microsphere that can be calculated if the stiffness of the trap and the displacement of the microsphere are known (see section 2.7.3). Optical trap stiffness can be obtained using a variety of techniques, including the power spectral density method and the viscous drag force method [117]. One additional condition must be met to capture a microsphere: the objective lens must have a high numerical aperture and the microsphere must have a refractive index greater than that of the surrounding milieu.

Optically trapped microspheres have been used extensively in molecular mechanics studies. For example, many mechanical and kinetic properties, including binding force and step size, of the

motor protein kinase have been characterized by capturing kinesin-coated microspheres and manipulating their position such that they interact with microtubules [118-120]. Miyata *et al*. used an optical trap during an *in vitro* motility assay to estimate actin filament displacement by a single skeletal HMM molecule [121]. Briefly, microsphere surfaces were modified to facilitate the attachment of a single actin filament. The filament was brought into contact with a low concentration of HMM molecules on the surface of the coverslip through manipulation of the optically trapped microsphere. The HMM molecules began generating force and motion through cross-bridge cycling, causing the microsphere to be displaced a measurable distance from the trap center. However, this method was limited because, when working with such low myosin concentrations (necessary for minimizing the risk of multiple attached myosin heads), the actin filament would often diffuse away from the HMM molecules.

Finer *et al*. therefore refined this technique using a three-microsphere system to successfully measure the unitary step size and unitary force of skeletal HMM molecules (Figure 1.10) [122]. Briefly, an actin filament was attached to two N-ethylmaleimide myosin (NEM) surface-modified microspheres, which were then captured individually using two optical traps. Through manipulation of the optically trapped microspheres, the filament was pulled taut and brought into contact with the surface of a third microsphere (sprayed on the coverslip prior to the nitrocellulose coating), commonly referred to as a pedestal, and sparsely coated with HMM molecules. A quadrant detector was used to measure microsphere displacement following the initiation of cross-bridge cycling. Force was measured using a feedback system that kept microsphere position constant during myosin-actin interactions by sending the quadrant detector output signal to acousto-optic modulators capable of making rapid trap displacements. More specifically, the force generated by a single HMM molecule was equal and opposite to the force required to prevent the microsphere from moving, which in turn was directly proportional to trap displacement. The three-microsphere laser trap assay developed by Finer *et al*. remains a popular technique to assess myosin molecular mechanics and has been used in many studies to characterize the mechanical properties of myosin purified from different muscle types [25, 67], single-headed myosin [123] and myosin fragments (HMM and S1) [124].

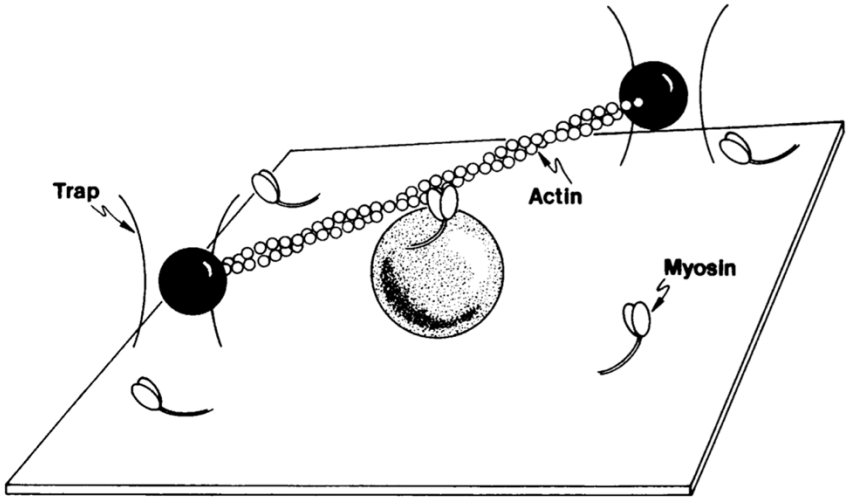

Figure 1.10: The three-microsphere laser trap assay. An actin filament is held taut and brought into contact with the myosin on a pedestal (speckled circle) by the micro-manipulation of two optically trapped microspheres (dark circles). The flow-through chamber coverslip is coated sparsely with myosin to ensure that single myosin-actin interaction events are observed (see text for details). Reproduced from [67]with permission from Elsevier.

Despite their effectiveness, present-day *in vitro* motility and laser trap assays are still limited. Dynamic studies, wherein the effects of altering assay conditions are observed in real-time, are infeasible due to the risk of interfering with the measurements themselves. To overcome this issue, Roman *et al*. developed a modified version of the conventional flow-through chamber that incorporated a microfluidic device to allow the diffusion of solutions during *in vitro* motility assays and laser trap assays without creating bulk flow [98]. However, the process required to manufacture the microfluidic device was lengthy and expensive. As such, a simplified version of this chamber was devised by replacing the glass coverslip with a plastic coverslip containing a through-hole covered by a microporous membrane to allow the diffusion of solutions during these assays [125]. These chambers constitute an important achievement towards performing dynamic *in vitro* motility and laser trap assays. However, major optimization is still required to reduce chemical diffusion time, minimize bulk flow and assure reproducibility of the results.

1.7 Thesis Rationale

The latch-state was studied thoroughly at the whole muscle level following its discovery in 1981 [71]. Several molecular mechanisms were proposed to explain this characteristic of smooth muscle, such as the formation of non-cycling or slowly cycling cross-bridges during LC_{20} dephosphorylation while myosin is attached to actin [71, 72, 74, 75], but none have been verified due to technological limitations. One such limitation was the inability to record molecular mechanics measurements while making dynamic changes to the conditions of *in vitro* motility and laser trap assays. An important step towards overcoming this obstacle was taken through the development of a flow-through chamber that permitted the diffusion of solutions during these assays [125]. However, the quality of the molecular mechanics measurements obtained using this version of the flow-through chamber were inconsistent. To this end, in the current study the design of the flow-through chamber was optimized and then used to perform *in vitro* motility and laser trap assays that reproduced the conditions for the latch-state at the molecular level. More specifically, MLCP was injected to induce LC_{20} dephosphorylation while recording force with the laser trap assay to verify if the latch-state could be reproduced at the molecular level. Furthermore, *in vitro* motility assay measurements were performed in the same conditions to assess the time-course of myosin deactivation. Finally, *in vitro* motility mixture assays with SKM, which does not deactivate by dephosphorylation, were also performed to assess for the potential formation of non-cycling, strong bonds. Verification of the latch-state at the molecular level is essential for understanding the fundamental properties of smooth muscle and may be clinically relevant to diseases associated with abnormal smooth muscle cell contraction, such as asthma and hypertension.

1.8 Thesis Objectives

The main goals of this thesis are to verify whether the latch-state can be reproduced at the molecular level and to understand the underlying molecular mechanisms that lead to the difference in force maintenance between tonic and phasic smooth muscle. To this end, the specific aims are as follows:

1. To optimize a flow-through chamber with chemical diffusion capabilities to recreate the conditions of the latch-state *in vitro* and allow for molecular mechanics measurements.

2. To measure the force generated by a population of phasic SMM or tonic SMM molecules pulling on an actin filament during LC_{20} dephosphorylation in the laser trap assay.
3. To measure the velocity and fraction of moving actin filaments being propelled by a population of phasic SMM or tonic SMM molecules during LC_{20} dephosphorylation in the *in vitro* motility assay.
4. To measure the velocity and fraction of moving actin filaments being propelled by a population of phasic SMM or tonic SMM molecules mixed with SKM molecules during (SMM) LC_{20} dephosphorylation in the *in vitro* motility mixture assay.

2 Materials & Methods

2.1 Reagents

The following reagents and chemicals were purchased from Sigma-Aldrich Canada: ATP (A3377), adenosine gamma-thio triphosphate (ATPγS) (A1388), BSA (A7030), $CaCl_2$ (C5080), catalase (C40), glucose (G7528), glucose oxidase (G2133-50KU), glycerol (356352), imidazole (I202), methylcellulose (M0512) and $MnCl_2$ (203734). The following reagents and chemicals were purchased from Fisher Scientific Canada: amylacetate (A718-500), DTT (BP172), EGTA (O2783), glutaraldehyde (BP25484), KCl (P330) and $MgCl_2$ (M33-500). Nitrocellulose (collodion) solution (53153, 5% stock) was purchased from Ladd Research Industries (Williston, VT).

2.2 Proteins

Tonic SMM (a gift from Dr. A. Sobieszek, Austrian Academy of Sciences) was purified from pig stomach fundus, whereas phasic SMM and SKM were purified from chicken gizzard and pectoralis respectively (obtained from a local slaughterhouse) [126]. MLCK and MLCP (gifts from Dr. A. Sobieszek, Austrian Academy of Sciences) were purified from turkey gizzard [127, 128]. Actin was purchased commercially (AKF99; Cytoskeleton, Denver, CO) and fluorescently labelled using tetramethyl rhodamine isothiocyanate (TRITC)-phalloidin (P1951; Sigma-Aldrich Canada) [70].

2.3 Buffers

Myosin buffer (300 mM KCl, 25 mM imidazole, 1 mM EGTA, 4 mM $MgCl_2$ and 15 mM DTT; pH adjusted to 7.4) and actin buffer (25 mM KCl, 25 mM imidazole, 0.1 mM $CaCl_2$, 4 mM $MgCl_2$, 15 mM DTT and an oxygen scavenger system consisting of 0.25 mg/mL glucose oxidase, 0.045 mg/mL catalase and 5.75 mg/mL glucose; pH adjusted to 7.4) were used for all experiments. The motility assay buffer consisted of actin buffer to which methylcellulose (0.5%), MgATP (2 mM) and $MnCl_2$ (1 mM; acts as a catalyst for MLCP) were added. The laser trap assay buffer consisted of actin buffer to which methylcellulose (0.3%), MgATP (200 μM) and $MnCl_2$ (1 mM) were added. The injection buffer consisted of actin buffer to which MgATP (2 mM), $MnCl_2$ (1 mM) and MLCP (1.5 μM) were added.

2.4 Myosin Phosphorylation

Phasic and tonic SMM were phosphorylated or thiophosphorylated according to Trybus *et al*. [32] with modifications. Phosphorylation and thiophosphorylation were performed in high salt conditions (HSC) for both phasic and tonic SMM, as well as low salt conditions (LSC) for tonic SMM only. Thiophosphorylated SMM, as well as tonic SMM phosphorylated in LSC, were only used during the optimization process (see section 2.8). All other experiments were performed exclusively with SMM phosphorylated in HSC.

Phasic SMM (HSC): Unphosphorylated phasic SMM (5 mg/mL) at high KCl (0.3 M) in modified myosin buffer (10x dilution with ddH_2O followed by the addition of DTT (30 mM final concentration)) was phosphorylated by incubation at room temperature for 20 min after the addition of the following: 6 mM $CaCl_2$, 3.75 μM calmodulin (P2277; Sigma-Aldrich Canada), 5 mM MgATP, 10 mM $MgCl_2$ and 0.07 μM MLCK. Glycerol (50% final concentration) and KCl (0.30 M final concentration) were added post incubation. The phosphorylated phasic SMM was then stored at -20°C and used within 72 h. Thiophosphorylation was performed in the same manner except that MgATP was substituted with magnesium-adenosine gamma-thio triphosphate (MgATPγS), the incubation period was changed to overnight at 4°C and the thiophosphorylated phasic SMM could be used for multiple months.

Tonic SMM (HSC): Unphosphorylated tonic SMM (5 mg/mL) at high KCl (0.3 M) in modified myosin buffer (10x dilution with ddH_2O followed by the addition of DTT (5 mM final concentration)) was phosphorylated by incubation at room temperature for 20 min after the addition of the following: 6.7 mM $CaCl_2$, 3 μM calmodulin, 5 mM MgATP, 10 mM $MgCl_2$ and 0.08 μM MLCK. Glycerol (50% final concentration) and KCl (0.30 M final concentration) were added post incubation. The phosphorylated tonic SMM was then stored at -20°C and used within 72 h. Thiophosphorylation was performed in the same manner except that MgATP was substituted with MgATPγS, the incubation period was changed to overnight at 4°C and the thiophosphorylated tonic SMM could be used for multiple months.

Tonic SMM (LSC): Unphosphorylated tonic SMM (5 mg/mL) in 10 mM KP_i, pH 7.5, 20 mM KCl, 1 mM EGTA, 2 mM NaN_3, 5 mM $MgCl_2$ and 1 mM DTT was phosphorylated by incubation at room temperature for 20 min after the addition of the following: 1.5 mM $CaCl_2$, 1.88 μM calmodulin, 1 mM MgATP, 1 mM $MgCl_2$ and 0.033 μM MLCK. Glycerol (50% final concentration) and KCl (0.30 M final concentration) were added post incubation. The phosphorylated tonic SMM was then stored at -20°C and used within 72 h. Thiophosphorylation was performed in the same manner except that MgATP was substituted with MgATPγS, the incubation period was changed to overnight at 4°C and the thiophosphorylated tonic SMM could be used for multiple months.

2.5 Assay Chamber

Flow-through chambers (10 μL) were constructed by securing a laser cut polyethylene terephthalate glycol (PETG) plastic coverslip (clear, 20 mm x 15 mm x 0.5 mm; Ponoko, San Francisco, CA) to a glass coverslip (Fisherbrand, 60 mm x 24 mm x 0.15 mm; Fisher Scientific Canada) coated in nitrocellulose (1.5% in amylacetate) using two pieces of double-sided tape (Scotch ATG 926, 6.4 mm x 0.13 mm; 3M, Grand Rapids, MI) laid in a parallel fashion approximately 2 mm apart using an adhesive applicator (Scotch ATG 714; 3M, St. Paul, MN). All buffers and proteins were flowed through the side openings between the plastic coverslip and glass coverslip. The plastic coverslip contained a through-hole (2 mm diameter) under which a hydrophilic, polycarbonate, microporous membrane (3 μm pore diameter; Sterlitech, Kent, WA)

was glued (NOA81; Norland Products, Cranbury, NJ) to allow for injection and diffusion of MLCP during the assay (Figure 2.1).

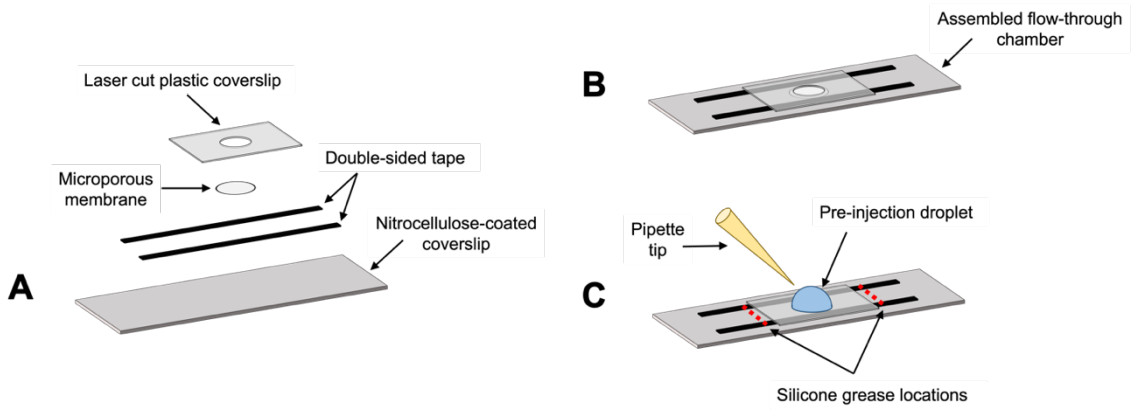

*Figure 2.1: Exploded (**A**) and assembled (**B**) views of the flow-through chamber used for all experiments. Dimensions are not to scale. A pre-injection droplet and silicone grease (**C**) were used to minimize bulk flow during MLCP injections performed with a pipette tip (see sections 2.6.1 and 2.6.3).*

2.6 *In Vitro* Motility and Mixture Assays

The *in vitro* motility assays (Figure 2.2) consisted of 100% phasic or tonic SMM, whereas the *in vitro* motility mixture assays consisted of 25% SKM and 75% phasic or tonic SMM; both were performed as described below.

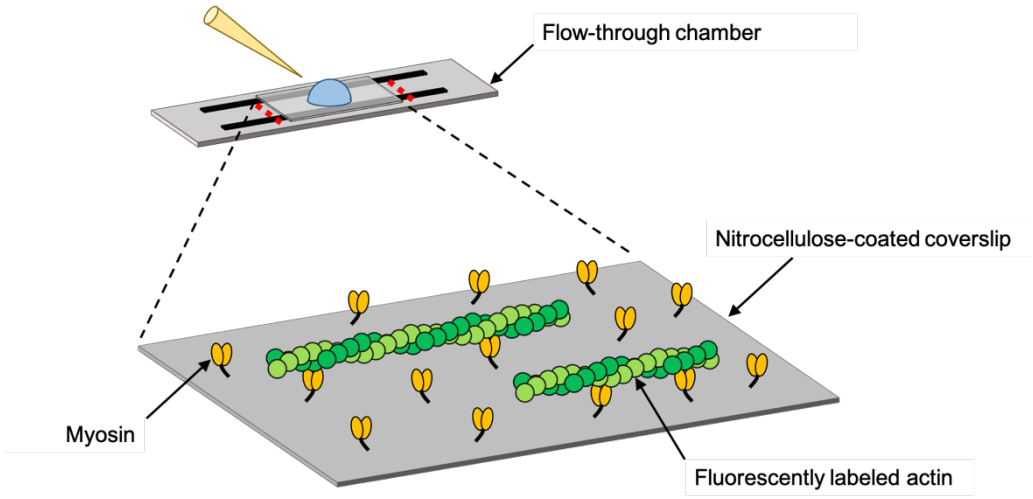

Figure 2.2: The in vitro motility assay performed with our novel flow-through chamber (see section 2.5). MLCP is injected on top of a pre-injection droplet (see section 2.6.3) and diffuses through

the microporous membrane of the flow-through chamber to dephosphorylate myosin molecules that are propelling fluorescently labeled actin filaments on a nitrocellulose-coated glass coverslip.

2.6.1 Assay Preparation

Non-functional myosin molecules were removed by ultracentrifugation (Optima L-90K ultracentrifuge, 42.2 Ti rotor, 31 min, 4°C, 42,000 rpm; Beckman Coulter, Fullerton, CA) of myosin (500 μg/mL) with filamentous actin (100 μg/mL) and MgATP (1 mM) in myosin buffer. The functional myosin was then diluted in myosin buffer to concentrations ranging between 75 μg/mL and 100 μg/mL (unless otherwise stated), perfused in the flow-through chamber and incubated for 2 min. Note that appropriate quantities of SKM and phasic or tonic SMM were mixed prior to dilution for the *in vitro* motility mixture assays [106]. This was followed by the addition of BSA (0.5 mg/mL in myosin buffer, two washes) and unlabeled G-actin (5 μM in actin buffer, two washes), incubated for 1 min and used to bind any remaining non-functional myosin. MgATP (1 mM in actin buffer, two washes) was then perfused to remove the unlabeled G-actin from the functional myosin, followed by actin buffer (two washes), TRITC-labeled actin (60 nM in actin buffer) incubated for 1 min, and motility assay buffer. High vacuum silicone grease (Z273554, Dow Corning; Sigma-Aldrich Canada) was then used to seal the side openings of the flow-through chamber to further minimize bulk flow, as well as to secure the flow-through chamber to a metal frame for structural support.

2.6.2 Data Acquisition

The flow-through chamber was then transferred to the stage of an inverted microscope (Eclipse Ti; Nikon Instruments, Melville, NY) equipped with a high numerical aperture objective (CFI Plan Fluor DLL 100XA, oil immersion, 1.3 numerical aperture; Nikon Instruments, Melville, NY). An objective lens heater (Bioptechs, Butler, PA) and heated microscope slide holder (Chamlide TC; Quorum Technologies, Puslinch, ON) were used to ensure that all experiments were conducted at 30°C. Actin filament movement was visualized and recorded using an excitation light source (X-Cite 120Q; Excelitas Technologies, Mississauga, ON), image intensified video camera (KP-E500 CCD, 720 x 480 resolution, 68.6 μm x 45.7 μm real frame size, 30 frames/s, 8-bit grayscale; Hitachi Kokusai Electric, Woodbury, NY) and custom software with a frame grabber

(MOR/2VD/84, Matrox). The average velocity (v) of all filaments moving faster than a cut-off velocity of 0.2 μm/s and motile fraction (f_{mot}) (the percentage of filaments moving above the same threshold) were measured using customized Matlab (version R2016b) video analysis software [100].

2.6.3 MLCP Injections

Immediately after transferring the flow-through chamber to the microscope stage, a 5 μL droplet of injection buffer lacking MLCP was placed on top of the microporous membrane. Injections of MLCP (5 μL of injection buffer) were performed using a 200 μL pipette tip connected to a glass, Luer lock syringe (25 μL; McMaster-Carr, Elmhurst, IL) by polyethylene tubing (1.6 mm inside diameter; McMaster-Carr, Elmhurst, IL) filled with water. An air gap of ~5 cm was left at the end of the tube connected to the pipette tip to prevent the water from mixing with the injection buffer. A transparent, acrylic plastic (McMaster-Carr, Elmhurst, IL) cover containing a small, angled through-hole (45°) was placed on top of the heated slide holder and secured with microscope stage clips to support the pipette tip during injections (Figure 2.3). The pipette tip was positioned directly above the droplet on the microporous membrane, without touching the droplet, to prevent early diffusion of MLCP. Baseline motility was recorded for approximately 30 s prior to injection.

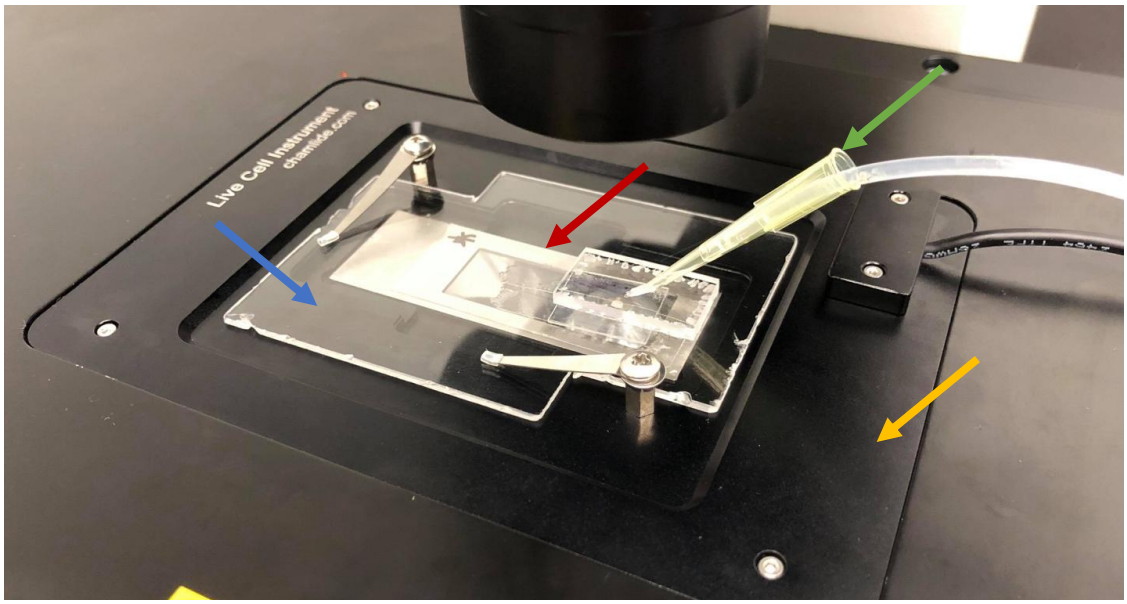

Figure 2.3: The experimental setup used for the laser trap and in vitro motility assays. A flow-through chamber is secured to a metal frame (red arrow), placed on the heated microscope slide

holder (yellow arrow), and then positioned such that the region below the microporous membrane is located directly above the objective lens. An acrylic plastic cover (blue arrow) is used to support the pipette tip (green arrow) during injections (see text for details).

Notably, a small decrease in *v* was usually observed after an injection was performed during the *in vitro* motility assays (Figure 2.4A). These decreases are thought to be artifacts because they occurred immediately at the time of injection, as well as when solutions other than MLCP were injected. The cause of these artifacts is unknown but is presumably related to trace amounts of convection or an optical effect.

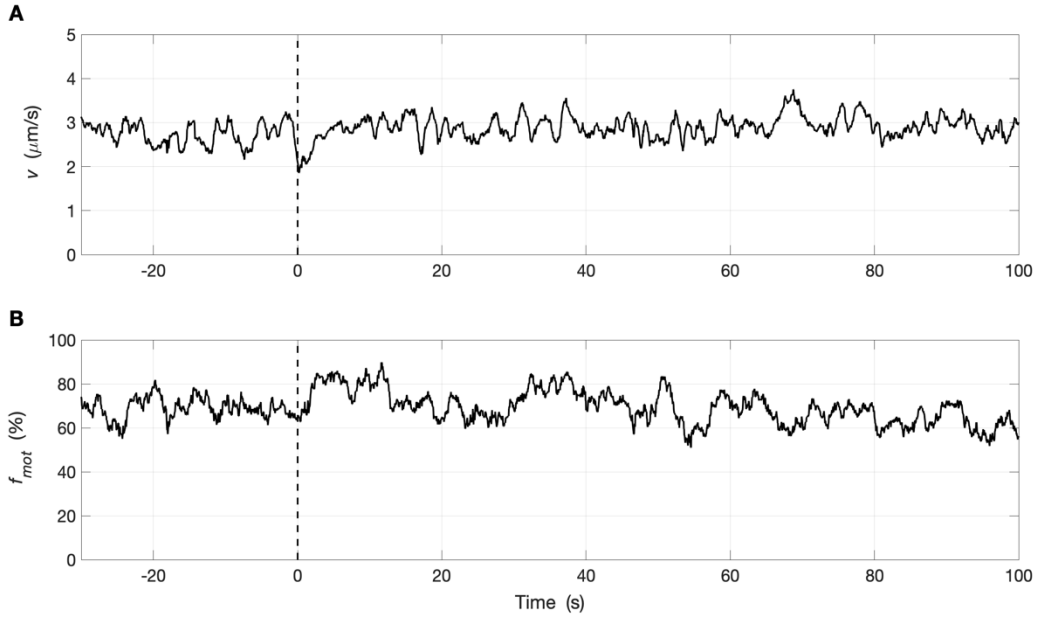

Figure 2.4: Representative in vitro motility assay data (SKM, n = 1) demonstrating the post-injection artifact. Actin buffer was injected at time = 0 s (dotted black lines), after which a small, brief drop in ***(A)*** *v and increase in* ***(B)*** f_{mot} *were observed (see text for details).*

2.6.4 Data and Statistical Analysis

The *In Vitro* Motility Assay: To quantify the time course of dephosphorylation in the *in vitro* motility assay, the f_{mot} and *v* data were fitted by a piecewise model consisting of three phases (Figure 2.5A, B) [125]. The first and third phases were both defined by constants, whereas the second phase was defined by a linear decrease:

$$f(t) = \begin{cases} y_1 & t < t_1 \\ \dfrac{y_2 - y_1}{t_2 - t_1} \cdot t + \left[y_1 - \dfrac{y_2 - y_1}{t_2 - t_1} \cdot t_1 \right] & t_1 \leq t < t_2 \\ y_2 & t \geq t_2 \end{cases} \quad (1)$$

where t is time, y_1 and y_2 are the values of f_{mot} or v during the first and third phases respectively, and t_1 and t_2 are the times at which the second phase starts and ends respectively. When fitting the data, only post-injection frames were included to eliminate the impact of the post-injection artifact (see section 2.6.3) on the model accuracy. To improve the accuracy of the model further, y_2 was set to zero when fitting the f_{mot} data as a means of reducing the impact of the noise following the end of the linear decrease. Filament motion was defined as stopped when $f_{mot} < 0.1$ and as such, f_{mot} and v data below this threshold were excluded from the model. t_1 and t_2 were determined exclusively with f_{mot} data because the signal-to-noise ratio observed was comparatively lower than in the v data. Thus, t_1 and t_2 for v were set to be equal to those estimated for f_{mot}.

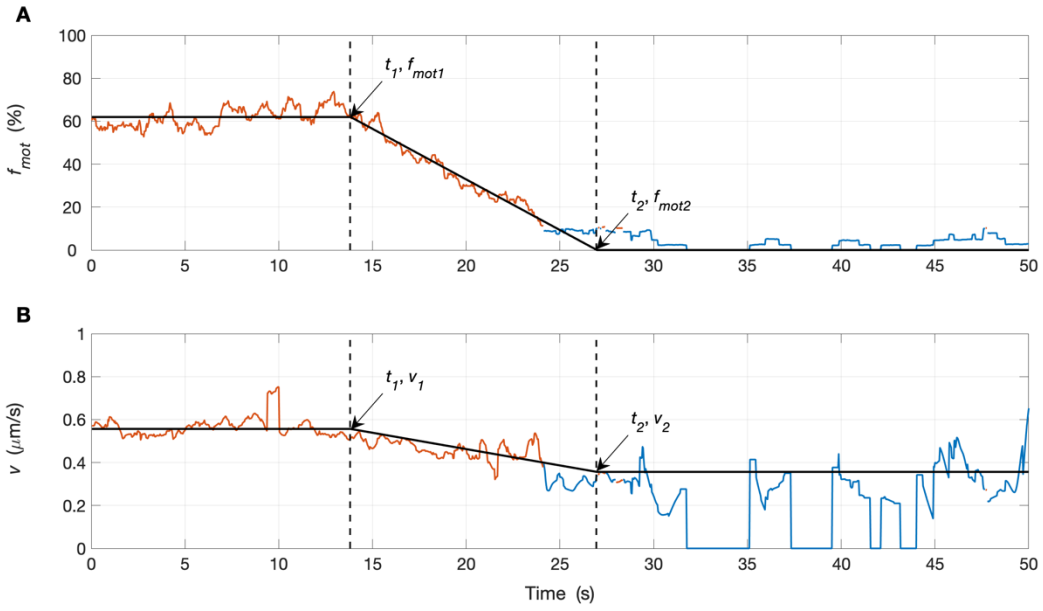

Figure 2.5: Representative in vitro motility assay data (phasic SMM, n = 1) fitted with ***(A, B)*** *the piecewise model (Eq. 1). Orange lines: data included in parameter optimization; blue lines: excluded data ($f_{mot} < 0.1$); solid black lines: the model. MLCP was injected at time = 0 s.*

y_1, y_2, t_1 and t_2 were determined for each trial individually by minimizing the root mean-squared error between the model and data using the *fminsearch* function in Matlab (version R2016b); each of these parameters was then averaged across all trials. For clarity, y_1 and y_2 are represented by f_{mot1} and f_{mot2} respectively for the f_{mot} data and by v_1 and v_2 respectively for the v data. The rate of change in f_{mot} (m_{fmot}) and the rate of change in v (m_v) during the second phase were determined for each trial individually by taking the difference between y_1 and y_2 normalized with respect to y_1 and then dividing it by the difference between t_1 and t_2. m_{fmot} and m_v were then averaged across all trials. Differences in these values between tonic SMM and phasic SMM were tested using the Student t-test where a value of $p < 0.05$ was considered significant. Data are reported as mean ± standard deviation (SD). n = 1 refers to a single flow-through chamber in which measurements were recorded at one location containing between ~20 and ~100 total (moving and stopped) filaments.

The *In Vitro* Motility Mixture Assay: To quantify the time course of dephosphorylation in the *in vitro* motility mixture assay (Figure 2.6A, B), the v data were fitted in the same way as described for the *in vitro* motility assay with the following exceptions: the second phase of the piecewise model (Eq. 1) was defined by a linear increase and both t_1 and t_2 were determined exclusively using v data because the phases described by the piecewise model were not observed in the f_{mot} data. Thus, t_1 and t_2 for f_{mot} were set to be equal to those estimated for v, and f_{mot1} and f_{mot2} were simply defined as the value of f_{mot} at t_1 and t_2 respectively. Additionally, m_{fmot} was determined by using the *polyfit* function in Matlab (version R2016b) to calculate the slope of the line of best fit (method of least squares) through the f_{mot} data, normalized with respect to f_{mot1}, between t_1 and t_2. Note that y_1, y_2, t_1, t_2, m_v and m_{fmot} were determined for each trial individually and then averaged; differences in these values between the tonic-skeletal mixture and the phasic-skeletal mixture were tested using the Student t-test where a value of $p < 0.05$ was considered significant. Data are reported as mean ± SD. n = 1 refers to a single flow-through chamber in which measurements were recorded at one location containing between ~50 and ~100 total (moving and stopped) filaments.

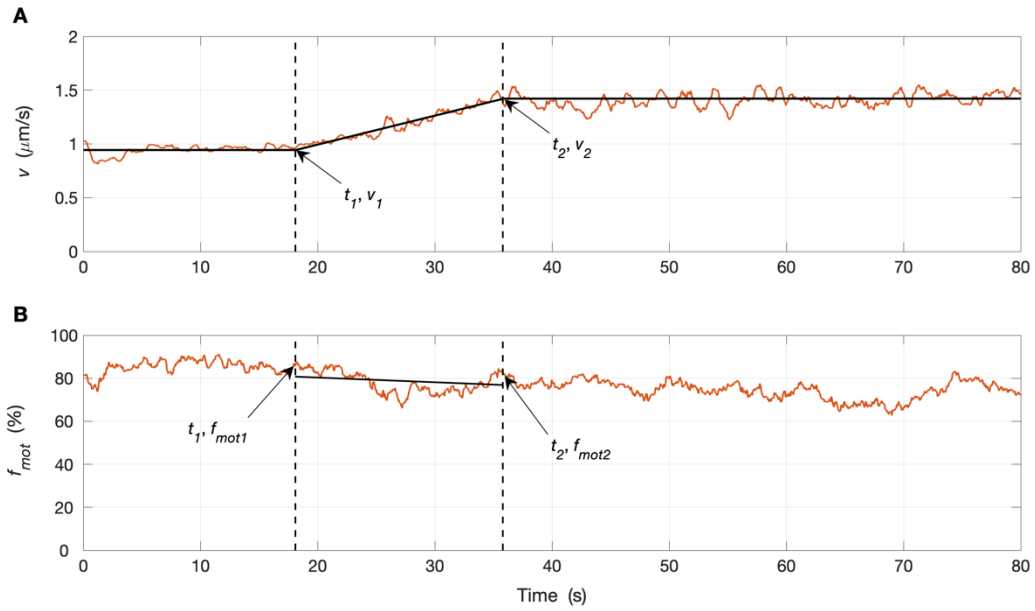

Figure 2.6: Representative in vitro motility mixture assay data (phasic SMM mixed with SKM, n = 1) fitted with ***(A)*** *the piecewise model (Eq. 1) and* ***(B)*** *the linear least squares model. Orange lines: data included in parameter optimization; solid black lines: the model. MLCP was injected at time = 0 s.*

2.7 Laser Trap Assay

An optical tweezers system was purchased commercially (MMI CellManipulator Plus; Quorum Technologies, Puslinch, ON) and combined with a modified version of the *in vitro* motility assay to create a single beam laser trap assay (Figure 2.7) that was used to obtain all force measurements as described below.

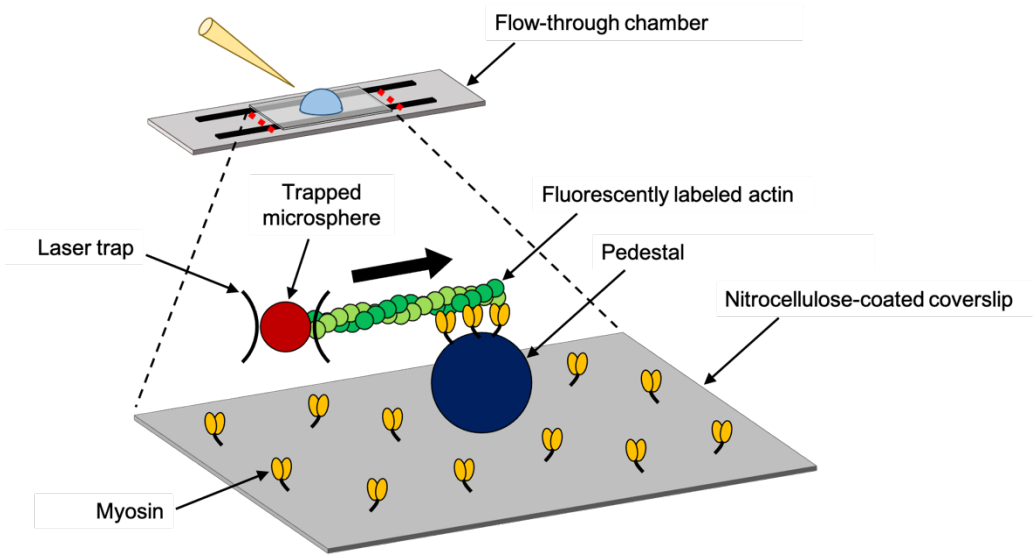

Figure 2.7: The laser trap assay performed with our novel flow-through chamber (see section 2.5). A microsphere (red) with an actin filament attached by the tail (see section 2.7.1) is captured in the laser trap and micro-manipulated to bring the actin into contact with the myosin on a pedestal (blue microsphere). MLCP is injected on top of a pre-injection droplet (see section 2.6.3) and diffuses through the microporous membrane of the flow-through chamber to dephosphorylate the myosin during isometric force generation by the myosin on the pedestal. Trap stiffness, measured using the Stokes force approach (see section 2.7.3), is multiplied by the distance that the microsphere is pulled away from the center of the trap (see section 2.7.2) to obtain force.

2.7.1 Assay Preparation

Before coating with nitrocellulose, the glass coverslips were sprayed with 4.5 µm polystyrene microspheres (171355, Polybead; Polysciences, Warrington, PA) to create pedestals [59]. Trapping was performed with 3 µm amino polystyrene microspheres (171455, Polybead; Polysciences, Warrington, PA) coated with gelsolin (G8032; Sigma-Aldrich Canada) according to Suzuki *et al*. [129] except that the time of suspension/gentle mixing of the microspheres in glutaraldehyde was increased to 15 h and the amount of protein dissolved in 0.5 mL of solution B was 27 µg gelsolin, 424 µg BSA and 27 µg G-actin. An Ytterbium infrared laser (8 W, 1070 nm) was used to create the trap. Proteins and solutions were prepared and perfused in the flow-through chamber in the same manner as for the *in vitro* motility assay, with the exception that (gelsolin-coated) microsphere-tailed actin filaments were added to the laser trap assay buffer. The

microsphere-tailed actin filaments were prepared according to Suzuki *et al*. [129] with the following modifications: only 5 μM TRITC-labeled actin were used and the suspension was diluted 1:10 with laser trap assay buffer to be perfused in the flow-through chamber.

2.7.2 Data Acquisition

The trapping microspheres were visualized in bright field (Figure 2.8A) by a charge-coupled device (CCD) camera (MXF285c, MMI CellCamera; Quorum Technologies, Puslinch, ON) and a single one was captured in the laser trap. An actin filament attached to the microsphere was visualized by fluorescence imaging (Figure 2.8B) as for the motility assay and then brought into contact with myosin molecules adhered to a pedestal. The myosin molecules then pulled on the actin-microsphere system and the injection of MLCP (see section 2.6.3) was performed once isometric force was reached. The force (*F)* exerted by the myosin on the actin-microsphere system was calculated as follows:

$$F = k \times \Delta x \qquad (2)$$

where k is the trap stiffness and Δx is the distance that the microsphere is pulled away from the center of the trap. Δx was calculated using custom Matlab video analysis software [59], whereas k was calibrated using the Stokes force method (see section 2.7.3) [130].

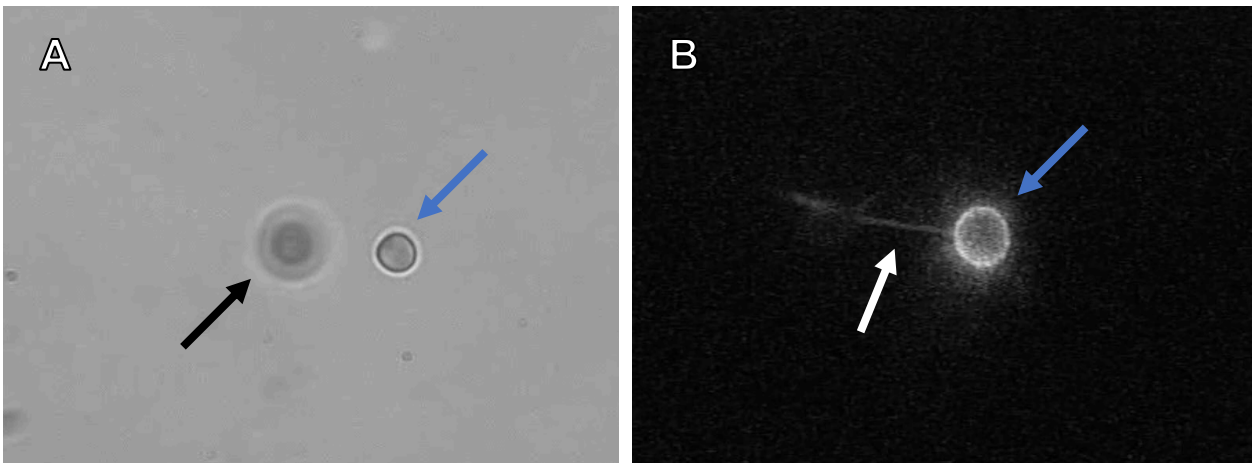

Figure 2.8: Bright field ***(A)*** *and fluorescence* ***(B)*** *images taken during the laser trap assay wherein the myosin (not visible) on a pedestal (black arrow) are pulling on a fluorescently labeled actin filament (white arrow) attached to a trapped microsphere (blue arrows). The myosin, pedestal and*

*trapped microsphere are not fluorescently labeled; the outline of the trapped microsphere is visible in image **B** because of small pieces of attached fluorescently labeled actin.*

2.7.3 Stiffness Calibration

While measuring Δx, a viscous drag (F_f) was applied to a trapped microsphere by moving it at a constant velocity (v_c) in water (water was used because its dynamic viscosity was more consistent than that of the laser trap assay buffer). F_f was then calculated as follows:

$$F_f = 6\pi\eta r v_c \qquad (3)$$

where η is 0.797 mPa·s, the dynamic viscosity of water at 30°C [131], and r is the radius of the microsphere. Thus, k can be calculated as follows:

$$k = {F_f}/{\Delta x} \qquad (4)$$

The value of k for a given laser power (LP) was averaged from several measurements performed at different v_c (Figure 2.9A). Values of k were determined at different LP levels and used to create linear fits. The slopes of these fits were averaged to obtain an interpolation constant (k_c = 8.87 $pN \cdot \mu m^{-1} \cdot LP^{-1}$) (Figure 2.9B), which was used to calculate k for each individual laser trap assay as follows:

$$k = LP \times k_C \qquad (5)$$

Although the majority of the trials shown in Figure 2.9B (n = 1 refers to a single flow-through chamber) were completed in the flow-through chamber described in Figure 2.1, one was completed in a conventional flow-through chamber [70] constructed using a nitrocellulose-coated glass coverslip (Fisherbrand Premium, 22 mm x 22 mm x 0.15 mm; Fisher Scientific Canada), glass microscope slide (Fisherbrand Premium, plain, 75 mm x 25 mm x 1 mm; Fisher Scientific Canada) and double-sided tape to verify the robustness of the calibration protocol.

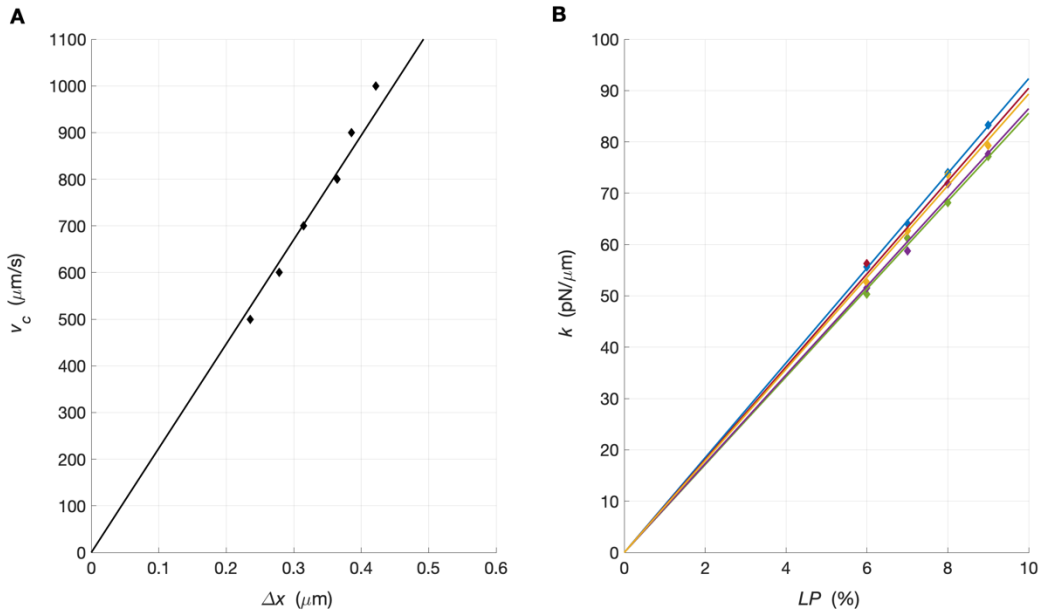

Figure 2.9: ***(A)*** *Laser trap stiffness calibration in water at 6% laser power (LP) (n = 1). Microsphere distance from the center of the trap (Δx) was measured (see section 2.7.2) as it was being moved at increasing velocity (v_c). Trap stiffness (k) was calculated at each v_c using the Stokes force exerted on the microsphere (Eq. 3, 4) and then averaged.* ***(B)*** *k was calibrated at increasing LP (6-9%) across multiple weeks. Linear fits were determined for each trial (n = 5), represented by different colours, and their slopes averaged to obtain an interpolation constant that was used to calculate k for each individual laser trap assay experiment (Eq. 5).*

2.7.4 Data and Statistical Analysis

The Laser Trap Assay: The time of injection following the start of force generation (T_{Inj}), the time during which force was maintained post-injection (T_{Hold}) and the average force post-injection were determined for each trial individually and then averaged. T_{Inj} was defined as the time pre-injection at which force started increasing and did not return to zero, whereas T_{Hold} was defined as the time post-injection until force reached and remained at zero. The average force post-injection was calculated during T_{Hold} for the MLCP-injection assays; for the control assays (see section 3.4.1), it was calculated during the average T_{Hold} of the MLCP-injection assays for either phasic or tonic SMM. Differences in T_{Inj} and T_{Hold} between phasic and tonic SMM for the MLCP-injection assays were assessed using the Student's t-test. Differences in T_{Inj} and T_{Hold} between the MLCP-injection assays and the control assays were assessed using the Mann-Whitney U-test. Differences

in the average force post-injection between phasic and tonic SMM, as well as between the MLCP-injection assays and the control assays, were assessed using the Student's t-test. $p < 0.05$ was considered significant for both the Student's t-test and Mann-Whitney U-test. Data are reported as mean ± SD and n = 1 refers to a single flow-through chamber.

2.8 Optimization

The *in vitro* motility and laser trap assays used in the current study are quite different from those previously described in the literature because of the need to diffuse MLCP during the measurements. The use of a flow-through chamber constructed with a plastic coverslip to accommodate a through-hole and a microporous membrane [125] required optimization to improve the quality of the molecular mechanics measurements. Note that these results are different from the scientific results of this study (see section 3) and as such, are presented in the methods for clarity.

2.8.1 *In Vitro* Motility Assay

Prior to optimization of the *in vitro* motility assay, the actin filaments were observed to be very short (Figure 2.10A). This suggested that myosin heads were degrading in the chamber and becoming non-functional (deadheads). Non-functional myosin is unable to hydrolyze MgATP and as such, does not detach from actin, leading to filament breakage and reductions in both f_{mot} and v (Figure 2.11A, C) [97]. The presence of deadheads in our assays is of major concern given that they could potentially contribute to false force maintenance results. To this end, many structural and biochemical changes were implemented to reduce the quantity of deadheads in both the *in vitro* and laser trap assays. The effectiveness of these changes was evaluated by measuring f_{mot}, v and the average length of stopped and moving filaments (L_f) [100] during a modified version of the *in vitro* motility assay wherein MLCP was not injected (from now on referred to as standard motility assays). The average f_{mot}, v and L_f were calculated over the interval 0 s < time < 30 s for each trial individually and then averaged. Differences in these values before and after optimization were tested using the Student t-test where a value of $p < 0.05$ was considered significant. Data are reported as mean ± SD. n = 1 is the same as described in section 2.6.4 except that the measurements were recorded at ~3 different locations in the flow-through chamber and then averaged.

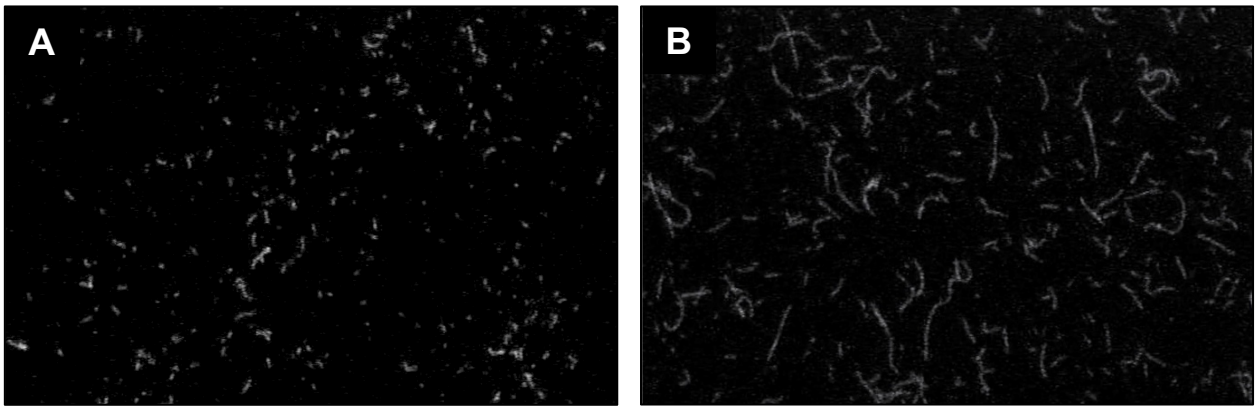

*Figure 2.10: Actin filaments observed by fluorescence imaging during standard myosin motility assays with **(A)** thiophosphorylated (HSC) tonic SMM in a conventional flow-through chamber (see section 2.7.3) prior to any optimization and **(B)** phosphorylated (HSC) tonic SMM in our novel flow-through chamber (see section 2.5) after optimization was completed (see text for details).*

Phase I: During this phase of optimization, the standard myosin motility assays were performed in conventional, glass flow-through chambers (see section 2.7.3) with thiophosphorylated tonic SMM to improve the quality of control molecular mechanics measurements. The effect of thiophosphorylating in both HSC and LSC conditions was assessed; it was found that these differences in thiophosphorylation conditions only affected the long-term conservation of the myosin and did not impact the quality of the measurements. Unlabeled G-actin perfused in the flow-through chamber was increased from 30 nM to 5 μM to improve the likelihood of binding deadheads that were not eliminated by ultracentrifugation and the concentration of TRITC-labeled actin perfused in the flow-through chamber was increased from 30 nM to 60 nM. The second of these changes was implemented to increase the signal-to-noise ratio of f_{mot} and v measurements by increasing the number of filaments available for averaging. After these changes were implemented, significant increases were observed for L_f (1.09 ± 0.25 μm versus 1.75 ± 0.20 μm; $p < 0.001$), f_{mot} (3.67 ± 1.21 % versus 51.80 ± 7.26 %; $p < 0.001$; Figure 2.11A, B) and v (0.19 ± 0.12 μm/s versus 0.59 ± 0.02 μm/s; $p < 0.001$; Figure 2.11C, D). Taken together, these results suggest that the first phase of optimization reduced the number of deadheads and increased the signal-to-noise ratio.

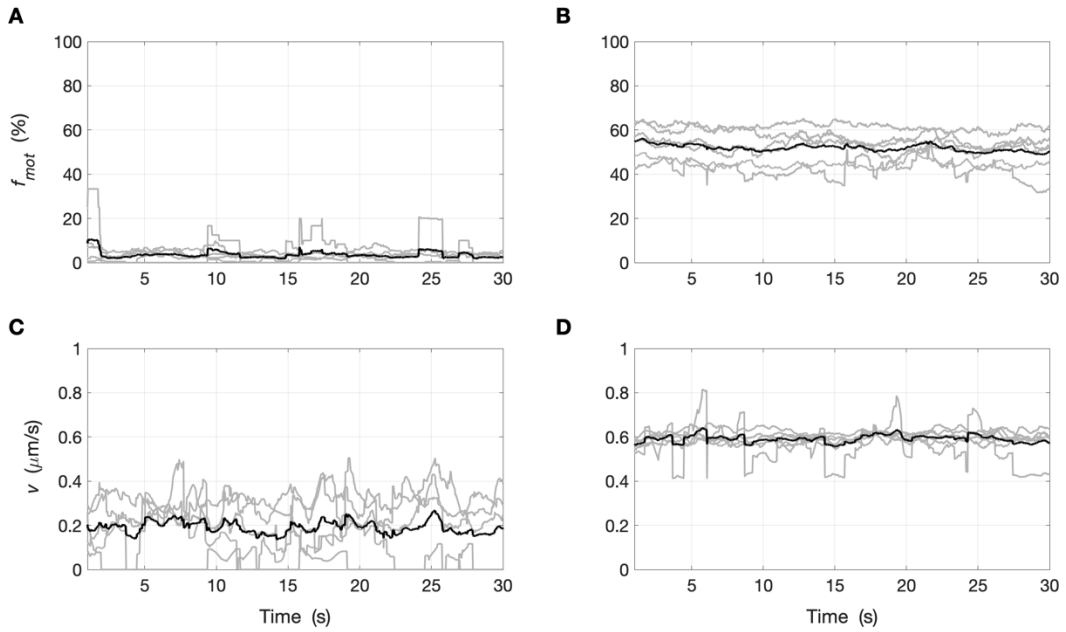

Figure 2.11: Phase I of optimizing the in vitro motility assay. ***(A, C)*** *Thiophosphorylated (HSC) tonic SMM (50-150 μg/mL) in standard myosin motility assays (n = 5) at the start of phase I.* ***(B, D)*** *Thiophosphorylated (HSC & LSC) tonic SMM (150 μg/mL) in standard myosin motility assays (n = 6) at the end of phase I. Assays were performed in conventional flow-through chambers (see section 2.7.3). Grey lines: data collected from a single assay; solid black lines: averaged data.*

Phase II: During this phase of optimization, the standard myosin motility assays were performed with phosphorylated tonic SMM (HSC and LSC) in the first version of our novel flow-through chamber [125] while incorporating the phase I protocol changes. Although v (0.62 ± 0.04 μm/s; Figure 2.12D) was not significantly different from that obtained in conventional flow-through chambers at the end of phase I (0.59 ± 0.02 μm/s; p = 0.202; Figure 2.11D), a significant decrease was observed for f_{mot} (51.80 ± 7.26 % versus 35.05 ± 6.88 %; p = 0.004; Figure 2.11B & Figure 2.12A) and a significant increase for L_f (1.75 ± 0.20 μm versus 2.17 ± 0.19 μm; p = 0.006). These results suggested that the myosin was distributing and adhering poorly to the nitrocellulose-coated glass coverslip, thus hindering actin filament propulsion.

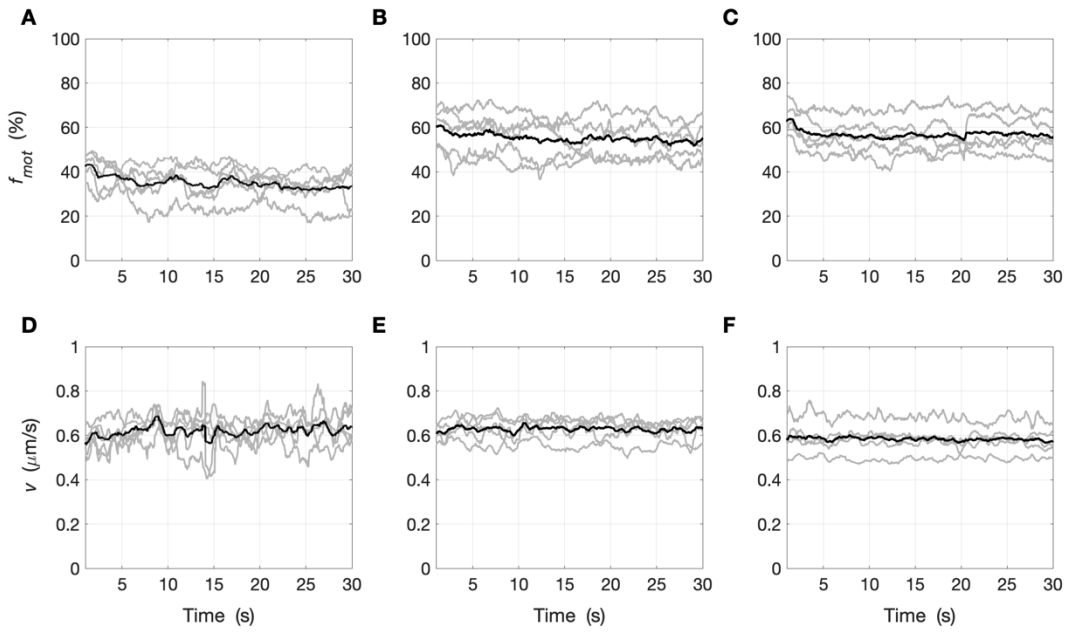

Figure 2.12: Phase II of optimizing the in vitro motility assay. ***(A, D)*** *Phosphorylated (LSC) tonic SMM (150 μg/mL) during standard myosin motility assays (n = 5) in our novel flow-through chamber at the start of phase II.* ***(B, E)*** *Phosphorylated (HSC) tonic SMM (90 μg/mL) during standard myosin motility assays (n = 5) in our novel flow-through chamber at the end of phase II.* ***(C, F)*** *Phosphorylated (HSC) tonic SMM (75-100 μg/mL) during standard myosin motility assays (n = 5) in our novel flow-through chamber after optimizing the MLCP injection protocol (see section 2.8.3). Grey lines: data collected from a single assay; solid black lines: averaged data.*

To overcome these issues, the plastic coverslip thickness was increased from 0.125 mm to 0.5 mm, increasing the flow-through chamber stiffness and potentially preventing turbulent flow development during perfusion. Additionally, the plastic coverslip through-holes were created using a laser cutter rather than a manual hole-puncher (Revolving Punch No. 223; C. S. Osborne & Co., Harrison, NJ) to eliminate the presence of deformed edges that were preventing the myosin from distributing properly underneath the microporous membrane. Although an exhaustive study of plastic biocompatibility was not performed, changing the material from polyester to PETG showed an improvement in f_{mot}. Lastly, the BSA coating step (see section 2.6.1) was performed in high ionic strength buffer (myosin buffer) rather than low ionic strength buffer (actin buffer) which appeared to decrease the number of deadheads. After these changes were implemented, a significant increase was observed for f_{mot} (35.05 ± 6.88 % versus 55.23 ± 9.14 %; p = 0.004; Figure

2.12A, B) but v (0.63 ± 0.05 μm/s; Figure 2.12E) was statistically the same as that obtained at the start of phase II (0.62 ± 0.04 μm/s; p = 0.782; Figure 2.12D). Furthermore, L_f (2.27 ± 0.26 μm) was also statistically the same as that obtained at the start of phase II (2.17 ± 0.19 μm; p = 0.509). Taken together, these results suggest that the second phase of optimization improved the uniformity of myosin distribution and adherence in the novel flow-through chamber, as well as reduced the number of deadheads.

2.8.2 Laser Trap Assay

Prior to optimization, two primary issues existed that prevented meaningful and reproducible laser trap assay data collection. The first was the presence of multiple actin filaments attached on individual microspheres, which made it difficult to ensure that the myosin heads on the pedestals were interacting with just one actin filament at any given time (Figure 2.13A). This was addressed by reducing the concentration of TRITC-labeled actin mixed with microspheres (see section 2.7.1) (Figure 2.13B).

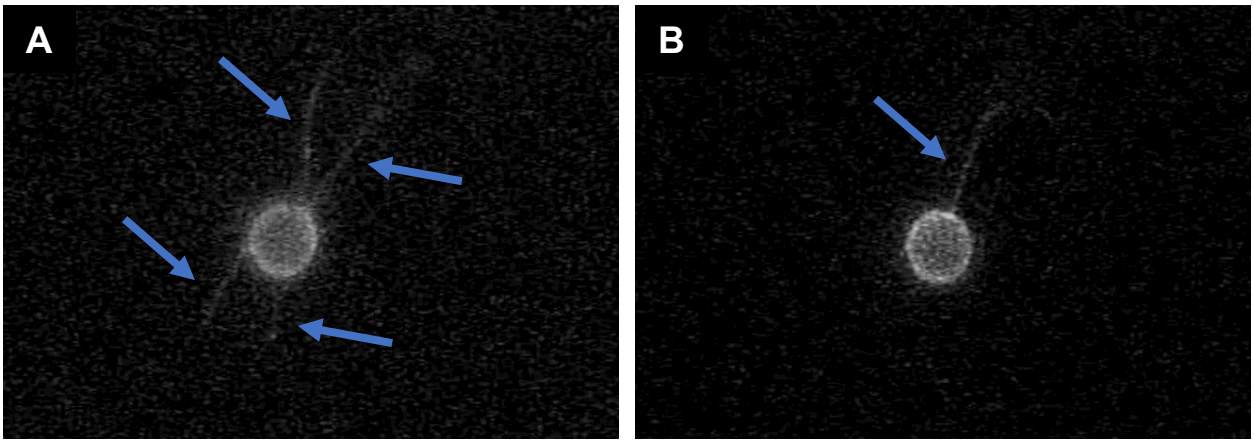

*Figure 2.13: Fluorescence images taken during laser trap assays wherein the trapped microsphere has **(A)** multiple filaments (blue arrows) attached to it and **(B)** one filament (blue arrow) attached to it.*

The second issue was the high frequency at which the actin-gelsolin bond was breaking once the myosin heads started pulling on the actin filament. To address this problem, the following changes were implemented: the concentration of myosin perfused in the flow-through chamber was

decreased from 125 μg/mL to a range between 75 μg/mL and 100 μg/mL as a means of reducing the force exerted on the actin-microsphere system; Ca^{2+} was added to the actin buffer to strengthen the binding between actin and the gelsolin-coated microspheres in the laser trap assay (see section 2.3) [129]. EGTA was thereafter eliminated from the actin buffer because it chelates Ca^{2+}.

2.8.3 Injection Protocol

Phase I: Due to the fragile nature of the microsphere-tailed actin filaments and the myosin-actin bonds during force measurements within the laser trap assay, it was imperative to reduce the diffusion time of MLCP through the membrane into the flow-through chamber as much as possible. To this end, membrane pore diameter was increased from 0.8 μm to 3 μm during phase II of the *in vitro* motility assay optimization. Prior to testing with MLCP, the effectiveness of this optimization was assessed by injecting MgATP (2 mM final concentration) in a modified *in vitro* motility assay containing actin filaments bound to myosin in rigor, and measuring the time elapsed before f_{mot} started increasing; differences in this value before and after optimization was tested using the Student t-test where a value of $p < 0.05$ was considered significant. Data are reported as mean ± SD. n = 1 is the same as described in section 2.6.4 except that the location where the measurements were recorded contained ~5 to ~10 filaments bound to myosin in rigor. These assays were prepared in the same manner as the *in vitro* motility assay, with the exception that the motility assay buffer and injection buffer did not contain MgATP. The time at which f_{mot} started increasing post-injection decreased significantly after implementing the aforementioned change (63.60 ± 1.10 s versus 11.67 ± 5.46 s; $p < 0.001$; Figure 2.14A, B).

Phase II: During the laser trap assay optimization, the injection protocol was modified to further minimize bulk flow. High vacuum silicone grease was used to seal the side openings of the flow-through chamber and injections were performed onto a 5 μL droplet rather than directly in the microporous membrane (see section 2.6.3). Following the implementation of these changes, the time at which f_{mot} started increasing post-injection increased significantly (11.67 ± 5.46 s versus 45.26 ± 5.58 s; $p < 0.001$; Figure 2.14B, C). To decrease this time once again, the plastic coverslip was placed on the double-sided tape such that the microporous membrane was facing the nitrocellulose-coated glass coverslip rather than the exterior of the flow-through chamber. Additionally, actin buffer replaced the laser trap assay buffer in the injection buffer because it is

less viscous. The implementation of these changes significantly reduced the time at which f_{mot} started increasing post-injection (45.26 ± 5.58 s versus 0.59 ± 0.27 s; $p < 0.001$; Figure 2.14C, D) and minimally impacted the quality of the molecular mechanics measurements; f_{mot} (56.84 ± 8.19 %; Figure 2.12C) was statistically the same as that obtained at the end of phase II of the *in vitro* motility assay optimization process (55.23 ± 9.14 %; $p = 0.778$; Figure 2.12B), as was v (0.63 ± 0.05 µm/s versus 0.58 ± 0.07 µm/s; $p = 0.267$; Figure 2.12E, F). L_f (1.79 ± 0.16 µm; Figure 2.10B) was statistically the same as that obtained at the end of phase I (1.75 ± 0.20 µm; $p = 0.718$).

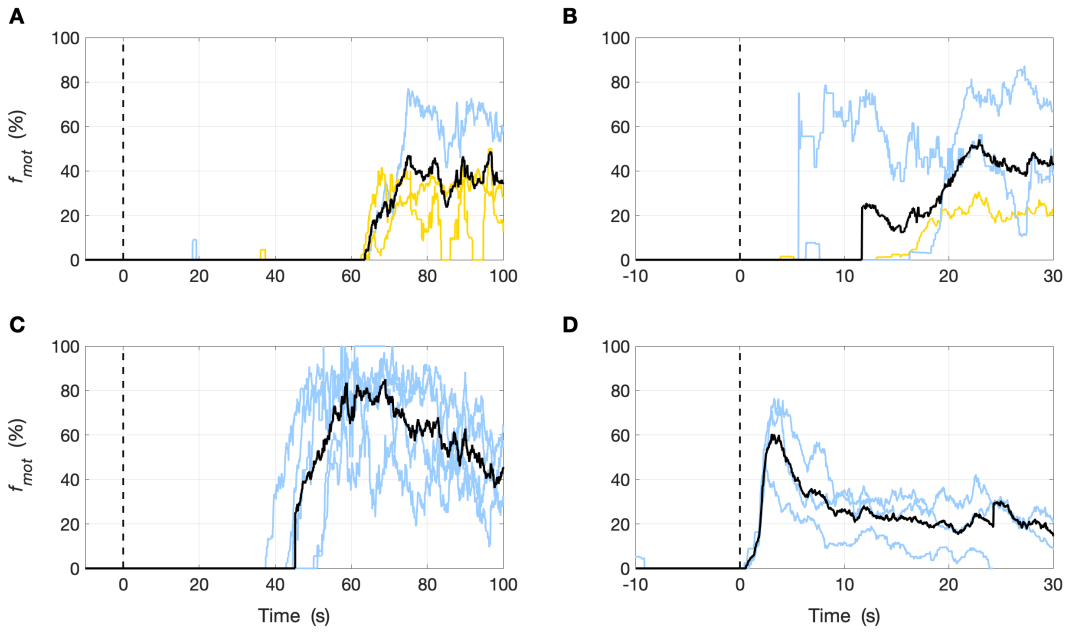

Figure 2.14: Phases I and II of optimizing the MLCP injection protocol; injection of MgATP during modified in vitro motility assays containing actin filaments bound to myosin in rigor. ***(A)*** *SKM (150 µg/mL, n = 1) and thiophosphorylated (HSC) phasic SMM (150 µg/mL, n = 2) at the start of phase I.* ***(B)*** *SKM (90 µg/mL, n = 2) and thiophosphorylated (HSC) phasic SMM (150 µg/mL, n = 1) at the end of phase I.* ***(C)*** *SKM (90 µg/mL, n = 5) at the start of phase II.* ***(D)*** *SKM (90 µg/mL, n = 3) at the end of phase II. Blue lines: data collected from a single assay performed with SKM; yellow lines: data collected from a single assay performed with SMM; solid black lines: averaged data; dotted black lines: time at which MgATP was injected.*

3 Results

3.1 SMM Dephosphorylation In The Laser Trap Assay

To verify whether force maintenance occurs during myosin LC_{20} dephosphorylation, MLCP was injected during laser trap assays performed with phasic or tonic SMM once the force generated by the myosin molecules had reached a plateau level. Both tonic SMM and phasic SMM showed force maintenance after the MLCP injection. Furthermore, the average force post-injection was not statistically different between tonic SMM and phasic SMM (51.03 ± 12.58 pN versus 48.85 ± 11.90 pN; p = 0.786). However, T_{Hold} was statistically greater for tonic SMM than phasic SMM (36.49 ± 11.53 s versus 20.96 ± 6.36 s; p = 0.030). Note that T_{Inj} was not statistically different between tonic SMM and phasic SMM (11.74 ± 1.62 s versus 12.27 ± 2.47 s; p = 0.699; Figure 3.1A, B & Table 3.3).

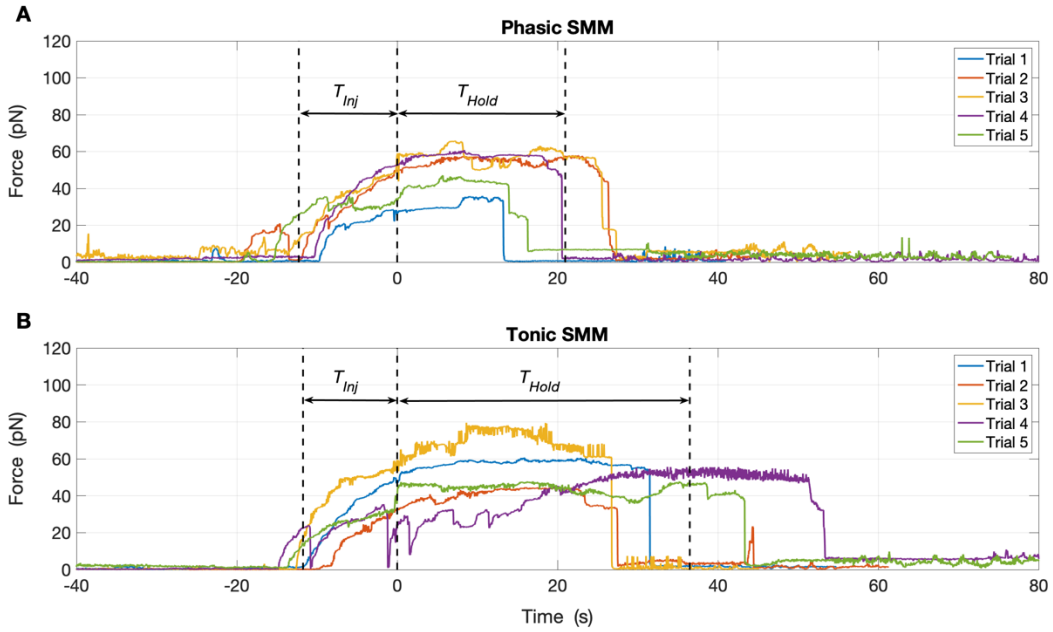

*Figure 3.1: Dephosphorylation of **(A)** phasic SMM (n = 5) and **(B)** tonic SMM (n = 5) during isometric force generation in the laser trap assay. Laser trap stiffness varied between 57.66 pN/µm and 62.10 pN/µm. MLCP was injected at time = 0 s. See section 3.4.1 for control injection data.*

3.2 SMM Dephosphorylation In The *In Vitro* Motility Assay

To elucidate the underlying mechanisms of the above results, as well as assess the time course of SMM deactivation, MLCP was injected during *in vitro* motility assays performed with phasic or tonic SMM. Tonic SMM was not statistically different from phasic SMM in terms of t_1 (17.31 ± 7.22 s versus 18.27 ± 4.75 s; p = 0.696), t_2 (39.09 ± 10.09 s versus 32.67 ± 7.13 s; p = 0.332) or m_{fmot} (-0.07 ± 0.05 s^{-1} versus -0.08 ± 0.02 s^{-1}; p = 0.939; Figure 3.2A-D & Table 3.1), suggesting that their respective dephosphorylation rates are similar.

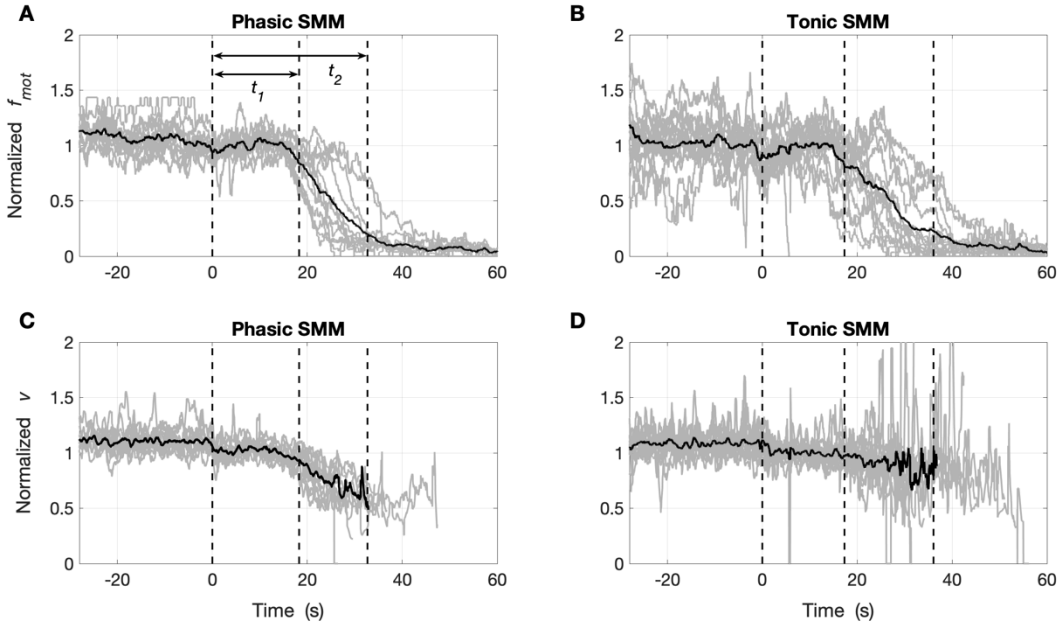

*Figure 3.2: Normalized f_{mot} and v during dephosphorylation of **(A, C)** phasic SMM (n = 12) and **(B, D)** tonic SMM (n = 15) in the in vitro motility assay. Grey lines: data collected from a single assay; solid black lines: averaged data. MLCP was injected at time = 0 s. Normalization was done with respect to the values at t_1. For clarity, v was not plotted past t_2.*

Interestingly, m_v was statistically less for tonic SMM than phasic SMM (-0.02 ± 0.02 s^{-1} versus -0.04 ± 0.02 s^{-1}; p < 0.001; Figure 3.2C, D & Table 3.1), suggesting that tonic SMM may cycle longer than phasic SMM following dephosphorylation. Together, these *in vitro* motility assay data show that the effect of MLCP on the mechanics of the myosin is observed starting ~17-18 s post-injection for both phasic and tonic SMM, which is within the range of T_{Hold} observed in the laser

trap assay for phasic SMM (20.96 ± 6.36 s; Figure 3.1A & Table 3.3) but less than T_{Hold} for tonic SMM (36.49 ± 11.53 s; Figure 3.1B & Table 3.3).

Table 3.1: The effects of injecting MLCP during in vitro motility assays performed with phasic SMM (n = 12) and tonic SMM (n = 15). m_{fmot} and m_v were determined using f_{mot} and v values normalized with respect to their values at t_1.

	t_1 (s)	t_2 (s)	f_{mot1} (%)	v_1 (μm/s)	v_2 (μm/s)	m_{fmot} (s^{-1})	m_v (s^{-1})
Tonic SMM	17.31 ± 7.22	39.09 ± 10.09	33.33 ± 10.72	0.46 ± 0.04	0.35 ± 0.10	-0.07 ± 0.05	-0.02 ± 0.02
Phasic SMM	18.27 ± 4.75	32.67 ± 7.13	65.50 ± 7.55	0.62 ± 0.08	0.29 ± 0.08	-0.08 ± 0.02	-0.04 ± 0.02
	p = 0.696	p = 0.332	p < 0.001	p < 0.001	p = 0.095	p = 0.939	p = 0.005

3.3 SMM Dephosphorylation In The *In Vitro* Motility Mixture Assay

To assess whether dephosphorylated cross-bridges generate a load by remaining attached to actin, MLCP was injected during *in vitro* motility mixture assays performed with phasic or tonic SMM mixed with SKM. The tonic-skeletal mixture was not statistically different from the phasic-skeletal mixture in terms of t_1 (24.33 ± 9.87 s versus 17.54 ± 7.99 s; p = 0.116; Figure 3.3A-D & Table 3.2), v_1 (0.88 ± 0.05 μm/s versus 0.91 ± 0.05 μm/s; p = 0.341; Table 3.2) and v_2 (1.37 ± 0.14 μm/s versus 1.37 ± 0.18 μm/s; p = 0.999; Table 3.2).

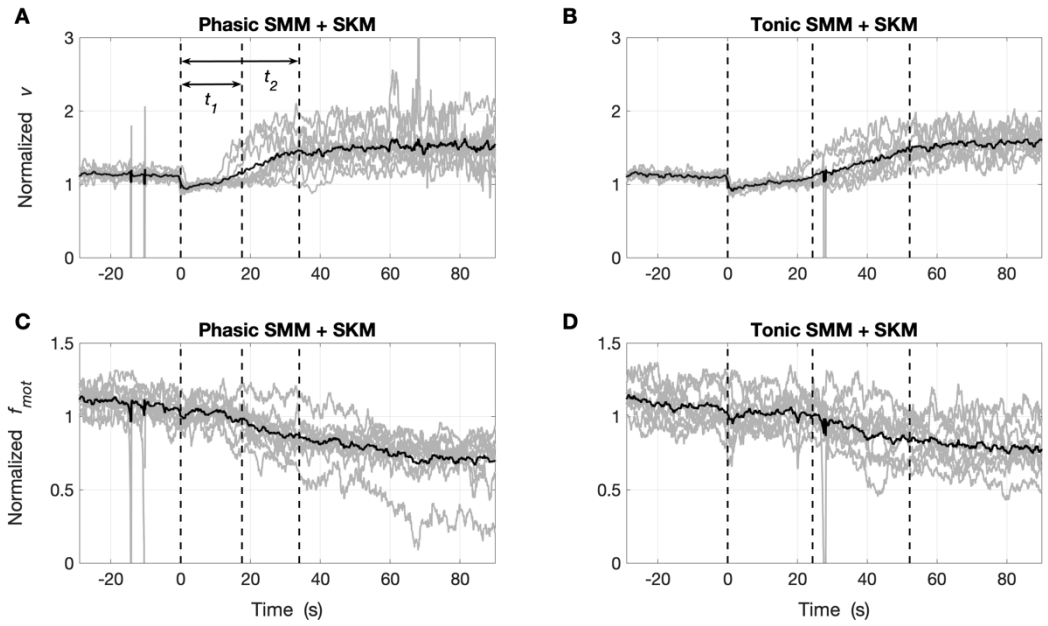

Figure 3.3: Normalized f_{mot} and v during dephosphorylation of ***(A, C)*** *phasic SMM when mixed with SKM (n = 10) and* ***(B, D)*** *tonic SMM when mixed with SKM (n = 9) in the in vitro motility mixture assay (75% tonic or phasic SMM: 25% SKM). Grey lines: data collected from a single assay; solid black lines: averaged data. MLCP was injected at time = 0 s. Normalization was done with respect to the values at t_1.*

A drop in v_1 would have been expected if a load had been generated but this was not observed, apart from an artifact at the time of injection observed for both the tonic-skeletal and phasic-skeletal mixtures (see section 2.6.3). However, t_2 occurred statistically later for the tonic-skeletal mixture than the phasic-skeletal mixture (52.18 ± 12.83 s versus 33.95 ± 13.56 s; p = 0.008), suggesting again that dephosphorylated tonic SMM continues cycling longer than dephosphorylated phasic SMM. m_v tended to be lower for the tonic-skeletal mixture than the phasic skeletal mixture, but this did not reach significance (0.02 ± 0.01 s^{-1} versus 0.04 ± 0.03 s^{-1}; p = 0.088). Similar to the *in vitro* motility assays, m_{fmot} was not statistically different between the tonic-skeletal mixture and the phasic-skeletal mixture (-0.01 ± 0.01 s^{-1} versus -0.01 ± 0.01 s^{-1}; p = 0.438; Figure 3.3C, D & Table 3.2). As expected, f_{mot} for the *in vitro* motility mixture assays did not decrease to the levels observed during the *in vitro* motility assays due to the presence of SKM continuing to propel the actin filaments.

Table 3.2: The effects of injecting MLCP during in vitro motility mixture assays (75% tonic or phasic SMM: 25% SKM) performed with phasic SMM when mixed with SKM (n = 10) and tonic SMM when mixed with SKM (n = 9). m_{fmot} and m_v were determined using f_{mot} and v values normalized with respect to their values at t_1.

	t_1 (s)	t_2 (s)	f_{mot1} (%)	f_{mot2} (%)	v_1 (μm/s)	v_2 (μm/s)	m_{fmot} (s^{-1})	m_v (s^{-1})
Tonic SMM + SKM	24.33 ± 9.87	52.18 ± 12.83	69.46 ± 4.93	57.04 ± 6.15	0.88 ± 0.05	1.37 ± 0.14	-0.01 ± 0.01	0.02 ± 0.01
Phasic SMM + SKM	17.54 ± 7.99	33.95 ± 13.56	74.51 ± 5.91	63.30 ± 7.77	0.91 ± 0.05	1.37 ± 0.18	-0.01 ± 0.01	0.04 ± 0.03
	p = 0.116	p = 0.008	p = 0.061	p = 0.070	p = 0.341	p = 0.999	p = 0.438	p = 0.088

3.4 Control Data

3.4.1 Control Data For The Laser Trap Assay

To verify that the abrupt drop in force observed after injecting MLCP (T_{Hold}) is not due to a physical disturbance caused by the injection itself, the laser trap measurements were repeated using injection buffer lacking MLCP (from now on referred to as control buffer). The average force post-injection was not found to be statistically different when injecting control buffer instead of MLCP for both tonic SMM (51.45 ± 13.11 pN versus 51.03 ± 12.58 pN; p = 0.960) and phasic SMM (44.74 ± 11.09 pN versus 48.85 ± 11.90 pN; p = 0.587). However, T_{Hold} was found to be statistically greater when injecting control buffer instead of MLCP for both tonic SMM (124.35 ± 97.43 s versus 36.49 ± 11.53 s; p = 0.016) and phasic SMM (117.16 ± 95.36 s versus 20.96 ± 6.36 s; p = 0.032). Note that T_{Inj} was not statistically different when injecting control buffer instead of MLCP for phasic SMM (18.65 ± 6.93 s versus 12.27 ± 2.47 s; p = 0.095; Figure 3.1A, Figure 3.4A & Table 3.3). However, T_{Inj} was statistically greater when injecting control buffer instead of MLCP for tonic SMM (22.90 ± 5.21 s versus 11.74 ± 1.62 s; p = 0.008; Figure 3.1B, Figure 3.4B & Table 3.3) but this difference in T_{Inj} of ~13s was very small compared to T_{Hold} of ~124 s. These results suggest that these abrupt decreases in force were real events induced by dephosphorylation and not simply artifacts.

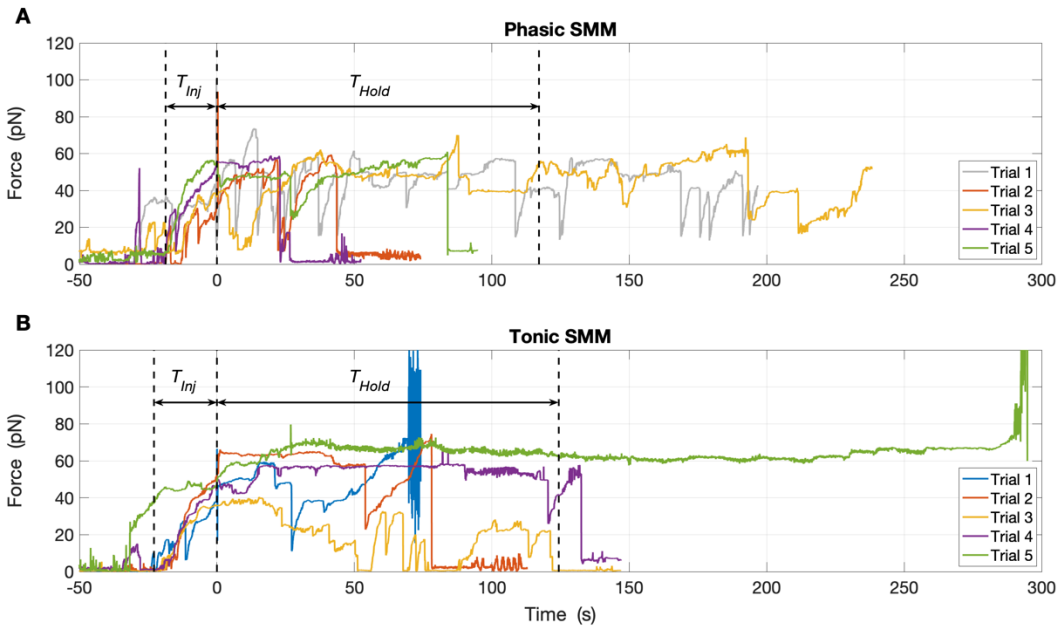

Figure 3.4: The effects of injecting control buffer during isometric force generation by ***(A)*** *phasic SMM (n = 5) and* ***(B)*** *tonic SMM (n = 5) in laser trap assays. Laser trap stiffness varied between 57.66 pN/μm and 70.97 pN/μm. Control buffer was injected at time = 0 s.*

The abrupt drops in force observed during MLCP injections (Figure 3.1A, B) occurred when myosin released the actin filament, as assessed by visual inspection of the fluorescence camera videos. Specifically, the actin filament remained bound to the gelsolin-coated microsphere and the microsphere itself remained in the trap. Conversely, most of the sudden drops in force observed during control buffer injections (Figure 3.4A, B) were due to the actin filament unbinding from the microsphere or the microsphere getting pulled out of the trap, except for trial 5 for phasic SMM (Figure 3.4A) and trials 2 and 4 for tonic SMM (Figure 3.4B). Lastly, the video recordings for both trials 1 and 3 for phasic SMM (Figure 3.4A) were manually stopped because the actin filament fluorescence had faded completely. Despite these artifacts, T_{Hold} was still found to be statistically longer when injecting control buffer instead of MLCP for both SMM types. Thus, MLCP leads to force decrease but this takes longer with tonic than phasic SMM.

Table 3.3: The effects of injecting MLCP or control buffer during isometric force generation by tonic SMM (n = 5) or phasic SMM (n = 5) in laser trap assays.

	Force (pN)	T_{Hold} (s)	T_{Inj} (s)		Force (pN)	T_{Hold} (s)	T_{Inj} (s)
Tonic MLCP	51.03 ± 12.58	36.49 ± 11.53	11.74 ± 1.62	Phasic MLCP	48.85 ± 11.90	20.96 ± 6.36	12.27 ± 2.47
Tonic Buffer	51.45 ± 13.11	124.35 ± 97.43	22.90 ± 5.21	Phasic Buffer	44.74 ± 11.09	117.16 ± 95.36	18.65 ± 6.93
	p = 0.960	p = 0.016	p = 0.008		p = 0.587	p = 0.032	p = 0.095

3.4.2 Control Data For The *In Vitro* Motility Mixture Assay

MLCP was injected during *in vitro* motility assays performed with SKM to assess for a potential effect on non-SMM. As expected, no statistical difference was observed in f_{mot} (66.67 ± 9.53 % versus 62.93 ± 8.23 %; p = 0.703; Figure 3.5A) or v (4.80 ± 0.70 μm/s versus 4.40 ± 0.72 μm/s; p = 0.278; Figure 3.5B) after MLCP was injected.

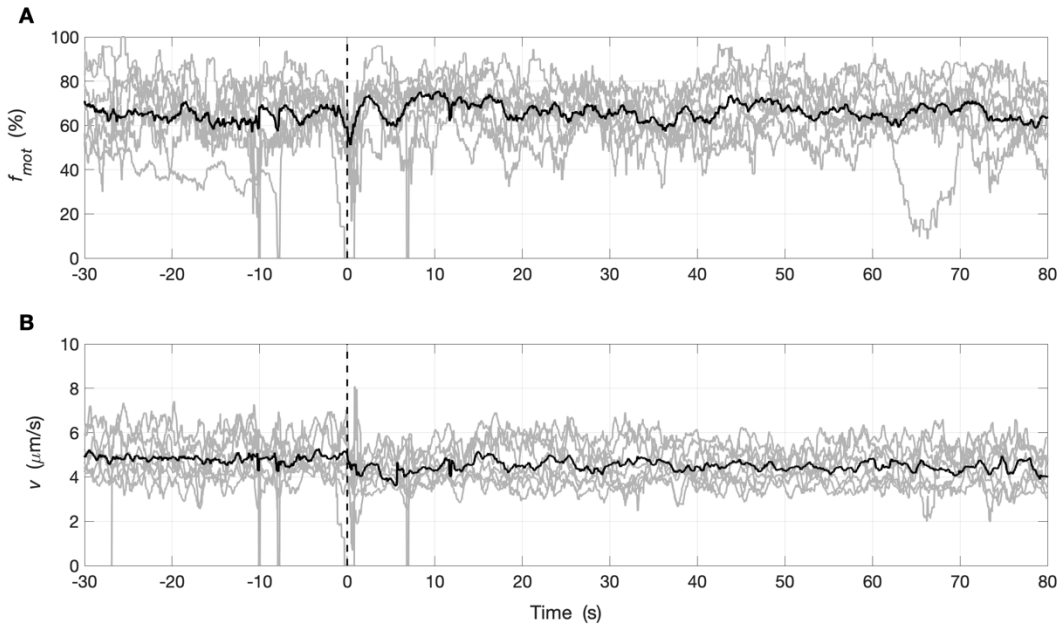

Figure 3.5: Injection of MLCP during in vitro motility assays performed with SKM (125 μg/mL, n = 8) in an earlier version of our novel flow-through chamber (see section 2.8.3). Grey lines: data collected from a single assay; solid black lines: averaged data; dotted black lines: time at which

MLCP was injected. The average pre-injection value of ***(A)*** f_{mot} *or* ***(B)*** v *was calculated over the interval -30 s < time < 0 s; the average post-injection value of* f_{mot} *or* v *was calculated over the interval 0 s < time < 80 s; differences in these values were tested using the Student t-test where a value of* $p < 0.05$ *was considered significant.*

Note that a small decrease in both f_{mot} and v is observed at the time of injection but is most likely the result of an imaging artifact (see section 2.6.3). Although an earlier version of our novel flow-through chamber was used to collect these data (see section 2.8.3), we do not expect that this would alter the results.

4 Discussion

In this study, the conditions for the latch-state were reproduced in the laser trap and *in vitro* motility assays and force maintenance was observed, for the first time, at the molecular level. Force maintenance was longer for tonic than phasic SMM and together, our results suggest that this is because tonic SMM continues cycling longer after dephosphorylation.

4.1 The Latch-State

Several molecular mechanisms have been proposed to explain the latch-state following its discovery in the 1980s. These mechanisms include: non-cycling or slowly cycling cross-bridges forming during LC_{20} dephosphorylation while myosin is attached to actin [71, 72], LC_{20} dephosphorylation reducing the rate of MgADP release from myosin and thus prolonging its attachment time to actin [74, 75]; dephosphorylated myosin reattaching to actin via a cooperative mechanism induced by the remaining phosphorylated myosin heads communicating through the thick filament or the actin regulatory proteins [77], *etc*. However, these mechanisms were proposed based on the results of tissue level studies and were never explored at the molecular level due to technological limitations. Although researchers have since revisited the latch-state following the development of the laser trap and *in vitro* motility assays, studies were still limited by the inability to record measurements while making dynamic changes to the assay conditions. More specifically, apart from a preliminary report from our lab [125], nobody has been able to induce LC_{20}

dephosphorylation, a key aspect of the latch-state, while measuring actomyosin mechanics. As such, the underlying molecular mechanism of the latch-state remains unverified.

4.2 SMM Dephosphorylation In The Laser Trap Assay

As predicted by tissue level and single molecule level measurements [25], the isometric force generated by tonic SMM was not different from that of phasic SMM. However, LC_{20} dephosphorylation during isometric force generation led to longer force maintenance (T_{Hold}) for tonic SMM than phasic SMM. This difference in T_{Hold} could not be explained by a difference in T_{Inj} as it was the same for both tonic and phasic SMM. Moreover, while the latch-state occurs with a greater propensity in tonic muscle, force maintenance is also seen in phasic muscle albeit to a lesser extent [132]. Thus, it is not surprising to also see some force maintenance by phasic SMM.

The manner in which the force eventually decreased after injecting MLCP was abrupt for both tonic SMM and phasic SMM, and was likely the result of an "avalanche" effect caused by the low myosin concentrations used in the laser trap assay [122]. Lauzon *et al*. demonstrated that the unitary force of both the (+)insert and (-)insert SMMHC isoforms is ~1 pN and its unitary displacement ~10 nm [25]. Since the average force post-injection was ~50 pN for both tonic SMM and phasic SMM, it is reasonable to assume that only ~50 myosin molecules were attached to the actin filament at any given time during the post-injection force plateau. Microsphere displacement from the laser trap center was typically ~1 μm. Thus, due to the restorative force of the trap on the microsphere, the disturbance of a single cross-bridge, due to Brownian motion for example, would be expected to cause the actin filament to slip by ~20 nm; it is possible that such a slip disrupted additional cross-bridges and led to the sudden, large drop in force. It is expected that in a muscle bundle, such slippage would be better compensated by the numerous other myosin-actin interactions.

It is worth noting that these abrupt decreases in force were also observed during the laser trap assays wherein control buffer was injected. However, in the absence of MLCP, the force could increase again following the sudden drops due to phosphorylated myosin molecules reattaching to the actin filament and preventing the "avalanche" effect from reaching completion. The fact that this reattachment occurred to the same extent with the phasic and tonic SMM in these control

experiments (similar T_{Hold}), but not during the MLCP injection experiments (different T_{Hold}), suggests that LC_{20} dephosphorylation has a different effect on tonic and phasic SMM.

4.3 SMM Dephosphorylation In The *In Vitro* Motility Assay

To elucidate the mechanism responsible for the force maintenance observed in the laser trap assay, MLCP was injected during *in vitro* motility assays performed with phasic SMM or tonic SMM. The observed decrease in f_{mot} and v confirmed the deactivation of the SMM by the MLCP injected into the flow-through chamber. It was necessary to verify this deactivation mechanically because measuring the phosphorylation level of such few myosin molecules with a gel is challenging. The lack of a difference in t_1, t_2 and m_{fmot} between phasic SMM and tonic SMM suggests that their dephosphorylation rates are of similar magnitude. It should be noted that after MLCP is injected during *in vitro* motility assays, actin filament motion transitions from directional to "wiggly" and stationary. Automated video analysis [100] interprets these "wiggly" filaments as having small directional movement and as such, f_{mot} never reached zero. To reduce the impact of this noise on the accuracy of the three-phase piecewise model, f_{mot2} was forced to zero when fitting the f_{mot} data (see section 2.6.4). To ascertain that this approach did not influence our results, we repeated the fits without constraining f_{mot2} and obtained similar m_{fmot}. Finally, the decrease in f_{mot} was also fitted exponentially and a similar time constant was obtained for the tonic and phasic SMM. Thus, the similarity of the rates of decrease in f_{mot} for tonic and phasic SMM suggests that their dephosphorylation rates are of similar magnitude. To our knowledge, the phosphorylation and dephosphorylation rates of tonic and phasic SMM have only been studied at the tissue level and the differences reported were attributed to differences in MLCK/MLCP ratios [77]. Comparatively, in our study the same concentration of MLCP led to a similar dephosphorylation rate, yet to a different T_{Hold}.

Given that tonic and phasic SMM dephosphorylate at a similar rate, the lower m_v observed for tonic SMM suggests again that the effect of LC_{20} dephosphorylation on tonic and phasic SMM is different. Indeed, the two-fold difference in m_v strongly suggests that dephosphorylated tonic SMM continues cycling longer than dephosphorylated phasic SMM. This is further supported by the fact that t_1, the time at which the mechanical effects of SMM dephosphorylation are first observed in the *in vitro* motility assay, is comparable to T_{Hold} in the laser trap assay for phasic

SMM (t_1 ~18 s versus T_{Hold} ~21 s) but less than that for tonic SMM (t_1 ~17 s versus T_{Hold} ~37 s). However, this is difficult to confirm because the "wiggly" behaviour of the actin filaments at low phosphorylation levels makes it challenging to measure v_2 precisely. Interestingly, the transition of v from clearly defined values to indistinct noise is abrupt for both the tonic and phasic SMM, and potentially more so for the tonic SMM. Indeed, v for the tonic SMM appears to decrease very little before the actin filament motion becomes too "wiggly" to measure accurately. This may occur because the dephosphorylated myosin has stopped cycling and only weak binding remains [31]. However, it could also be caused by the presence of a high load, such as attached, non-cycling cross-bridges [71, 72, 74, 75] that suddenly impedes actin filament motion.

4.4 SMM Dephosphorylation In The *In Vitro* Motility Mixture Assay

To determine whether a load is induced following SMM LC_{20} dephosphorylation, or if dephosphorylated tonic SMM indeed cycles longer than dephosphorylated phasic SMM, MLCP was injected during *in vitro* motility mixture assays performed with phasic SMM or tonic SMM mixed with SKM. Recall that SKM is not regulated at the thick filament level and as such, will continue cycling in the presence of MLCP. If non-cycling SMM cross-bridges had formed [71, 72, 74, 75], it follows that they would have imposed a load on the actin filaments being propelled by the still cycling SKM and thus, v_1 would have decreased. However, no such decrease was observed; the drop in v that occurred immediately after MLCP was injected was attributed to the artifact described in section 2.6.3 rather than a biological effect, as it occurred almost instantaneously with the injection for both the phasic-skeletal and tonic-skeletal mixtures. Interestingly, t_2 was longer for the tonic-skeletal mixture than the phasic-skeletal mixture, once again supporting the theory that tonic SMM continues cycling longer than phasic SMM during LC_{20} dephosphorylation. Consistent with these results, m_v showed a trend towards a two-fold difference between the tonic-skeletal mixture and the phasic-skeletal mixture. Although this difference did not reach significance, the reason can be attributed to the noise caused by small amounts of "wiggly" actin filament behaviour observed after SMM LC_{20} dephosphorylation.

It is interesting to note that after SMM dephosphorylation, v_2 did not reach the v expected for pure SKM (Figure 3.5B) but reached the same value for both the phasic-skeletal and the tonic-skeletal mixtures. This is unlikely to have been caused by non-cycling SMM cross-bridges [71, 72, 74, 75]

because a v_2 of ~1.37 μm/s was observed over more than 30 s across all trials, during which time actin filaments will have travelled at least ~41 μm across the motility surface. This distance is three orders of magnitude larger than the 10 nm unitary displacement of SMM and SKM [25, 67] and as such, it is unrealistic to expect that SMM cross-bridges would remain attached and non-cycling over that distance. Conversely, weak binding of unphosphorylated SMM to actin is a likely explanation as to why v_2 in both the phasic-skeletal and tonic-skeletal mixtures did not reach the level of SKM. Indeed, early mixture assays demonstrated that unphosphorylated SMM imposes a small load on actin filaments propelled by SKM, thereby reducing their velocity [70]. Moreover, single molecule level measurements showed that both unphosphorylated tonic and phasic SMM bind to actin with ~1/10 the amount of force generated by phosphorylated myosin [31], thereby explaining their similar effect in the *in vitro* motility mixture assays.

4.5 Additional Remarks

A few additional points are worth noting, the first being that the SMM molecules used in this study were not pure (+)insert or (-)insert SMMHC isoform preparations. Instead, myosin was purified from organs in which the smooth muscle exhibited mostly tonic and mostly phasic behaviors. While these SMM preparations are representative of real physiological systems, it made the results more challenging to interpret at times. For example, while v_1 is lower for tonic SMM than phasic SMM in the *in vitro* motility assay (Table 3.1), this difference is lost once the SMM is mixed with SKM in the *in vitro* motility mixture assay (Table 3.2). It is therefore remarkable that differences between phasic SMM and tonic SMM for T_{Hold} in the laser trap assay, m_v in the *in vitro* motility assay and t_2 in the *in vitro* motility mixture assay could still be observed, further supporting the robustness of these results.

Another point worth mentioning is that the purification of tonic SMM is inherently more difficult to accomplish than that of phasic SMM because of its longer attachment time to actin. Thus, f_{mot1} is lower for tonic SMM than phasic SMM in the *in vitro* motility assay (Table 3.1) due to the presence of some non-functional myosin molecules (deadheads). It is possible that, even with all the precautions taken (see section 2.8), some of these deadheads bound in rigor to actin and possibly contributed to the reattachment of dephosphorylated myosin as previously suggested [82]. However, this is unlikely to have contributed much to the results of this study because the strong

binding of deadheads to actin leads to actin filament breakage and this was not observed to a greater extent in the tonic SMM than the phasic SMM assays.

Lastly, although this thesis focused on the most basic theory of the latch-state with the minimum components needed for the cross-bridge cycle (myosin and actin), it will be easy in the future to investigate the role of the actin regulatory proteins by purifying whole thin filaments or decorating the actin filament with one protein type at a time. Furthermore, it will also be easy to alter the composition of the laser trap or motility assay buffer, such as by adding MgADP, to assess the role of different segments of the cross-bridge cycle in the latch-state.

5 Conclusion

A flow-through chamber that permits the diffusion of solutions during the laser trap and *in vitro* motility assays was successfully optimized such that robust actomyosin mechanics measurements could be recorded during LC_{20} dephosphorylation, marking an important advancement in the field of molecular mechanics measurements. Furthermore, force maintenance was observed for the first time at the molecular level, marking an important step towards elucidating the underlying molecular mechanisms of the latch-state. Taken together, the results of this study do not support the long-standing dogma of strong bonds caused by dephosphorylated, non-cycling cross-bridges leading to the latch-state. However, these results support the concept that LC_{20} dephosphorylation leads to slowly cycling cross-bridges and that this effect lasts longer for tonic than phasic SMM. This prolonged cycling of tonic SMM likely contributes to the longer force maintenance of tonic SMM compared to that of phasic SMM and thus, the greater propensity of tonic muscle to exhibit the latch-state. The reason why dephosphorylated tonic SMM may cycle for longer remains unclear and will require further investigations.

References

[1] B. M. Koeppen and B. A. Stanton, *Berne & Levy physiology*, Seventh edition. ed. Philadelphia, PA: Elsevier, 2018.

[2] L. S. Costanzo, *Physiology*, Sixth edition. ed. Philadelphia, PA: Elsevier, 2018.

[3] E. P. Widmaier, H. Raff, K. T. Strang, and A. J. Vander, *Vander's human physiology: the mechanisms of body function*, Fourteenth edition. ed. New York, NY: McGraw-Hill (in English), 2016.

[4] K. Mukund and S. Subramaniam, "Skeletal muscle: a review of molecular structure and function, in health and disease," (in eng), *Wiley Interdiscip Rev Syst Biol Med,* vol. 12, no. 1, p. e1462, Jan 2020, doi: 10.1002/wsbm.1462.

[5] J. G. Betts *et al.*, "Skeletal muscle," *Anatomy and Physiology*Houston, Texas: OpenStax, 2013, pp. 405-444. [Online]. Available: https://openstax.org/books/anatomy-and-physiology/pages/10-2-skeletal-muscle

[6] A. Weber, "On the role of calcium in the activity of adenosine 5'-triphosphate hydrolysis by actomyosin," (in eng), *J Biol Chem,* vol. 234, pp. 2764-9, Oct 1959.

[7] S. Ebashi, F. Ebashi, and A. Kodama, "Troponin as the Ca++-receptive protein in the contractile system," (in eng), *J Biochem,* vol. 62, no. 1, pp. 137-8, Jul 1967, doi: 10.1093/oxfordjournals.jbchem.a128628.

[8] A. F. Huxley and R. Niedergerke, "Structural changes in muscle during contraction; interference microscopy of living muscle fibres," (in eng), *Nature,* vol. 173, no. 4412, pp. 971-3, May 22 1954, doi: 10.1038/173971a0.

[9] H. Huxley and J. Hanson, "Changes in the cross-striations of muscle during contraction and stretch and their structural interpretation," (in eng), *Nature,* vol. 173, no. 4412, pp. 973-6, May 22 1954, doi: 10.1038/173973a0.

[10] H. E. Huxley, "The mechanism of muscular contraction," (in eng), *Science,* vol. 164, no. 3886, pp. 1356-65, Jun 20 1969, doi: 10.1126/science.164.3886.1356.

[11] A. Arner and U. Malmqvist, "Cross-bridge cycling in smooth muscle: a short review," (in eng), *Acta Physiol Scand,* vol. 164, no. 4, pp. 363-72, Dec 1998, doi: 10.1111/j.1365-201x.1998.tb10694.x.

[12] J. Ochala and Y.-B. Sun, "Novel myosin-based therapies for congenital cardiac and skeletal myopathies," *Journal of Medical Genetics,* vol. 53, no. 10, pp. 651-654, 2016, doi: 10.1136/jmedgenet-2016-103881.

[13] D. P. Wilson, "Vascular smooth muscle structure and function," in *Mechanisms of Vascular Disease: A Reference Book for Vascular Specialists*, R. Fitridge and M. Thompson Eds. Adelaide (AU): University of Adelaide Press

[14] J. Zhang, A. M. Herrera, P. D. Paré, and C. Y. Seow, "Dense-body aggregates as plastic structures supporting tension in smooth muscle cells," (in eng), *Am J Physiol Lung Cell Mol Physiol,* vol. 299, no. 5, pp. L631-8, Nov 2010, doi: 10.1152/ajplung.00087.2010.

[15] J. G. Betts *et al.*, "Smooth muscle," *Anatomy and Physiology*Houston, Texas: OpenStax, 2013. [Online]. Available: https://openstax.org/books/anatomy-and-physiology/pages/10-8-smooth-muscle

[16] E. Bosler, "Conduction, automaticity, and tonus of visceral muscles," (in eng), *Experientia,* vol. 4, no. 6, pp. 213-8, Apr 15 1948, doi: 10.1007/bf02155366.

[17] K. E. Creed, "Functional diversity of smooth muscle," (in eng), *Br Med Bull,* vol. 35, no. 3, pp. 243-7, Sep 1979, doi: 10.1093/oxfordjournals.bmb.a071584.

[18] H. L. Sweeney and A. Houdusse, "Structural and functional insights into the myosin motor mechanism," (in eng), *Annu Rev Biophys,* vol. 39, pp. 539-57, 2010, doi: 10.1146/annurev.biophys.050708.133751.

[19] K. M. Trybus, "Biochemical studies of myosin," (in eng), *Methods,* vol. 22, no. 4, pp. 327-35, Dec 2000, doi: 10.1006/meth.2000.1085.

[20] M. A. Geeves and K. C. Holmes, "Structural mechanism of muscle contraction," (in eng), *Annu Rev Biochem,* vol. 68, pp. 687-728, 1999, doi: 10.1146/annurev.biochem.68.1.687.

[21] R. Léguillette and A. M. Lauzon, "Molecular mechanics of smooth muscle contractile proteins in airway hyperresponsiveness and asthma," (in eng), *Proc Am Thorac Soc,* vol. 5, no. 1, pp. 40-6, Jan 1 2008, doi: 10.1513/pats.200704-053VS.

[22] G. J. Babu, D. M. Warshaw, and M. Periasamy, "Smooth muscle myosin heavy chain isoforms and their role in muscle physiology," (in eng), *Microsc Res Tech,* vol. 50, no. 6, pp. 532-40, Sep 15 2000, doi: 10.1002/1097-0029(20000915)50:6<532::Aid-jemt10>3.0.Co;2-e.

[23] S. White, A. F. Martin, and M. Periasamy, "Identification of a novel smooth muscle myosin heavy chain cDNA: isoform diversity in the S1 head region," (in eng), *Am J Physiol,* vol. 264, no. 5 Pt 1, pp. C1252-8, May 1993, doi: 10.1152/ajpcell.1993.264.5.C1252.

[24] R. Léguillette, F. R. Gil, N. Zitouni, S. Lajoie-Kadoch, A. Sobieszek, and A. M. Lauzon, "(+)Insert smooth muscle myosin heavy chain (SM-B) isoform expression in human tissues," (in eng), *Am J Physiol Cell Physiol,* vol. 289, no. 5, pp. C1277-85, Nov 2005, doi: 10.1152/ajpcell.00244.2004.

[25] A. M. Lauzon, M. J. Tyska, A. S. Rovner, Y. Freyzon, D. M. Warshaw, and K. M. Trybus, "A 7-amino-acid insert in the heavy chain nucleotide binding loop alters the kinetics of smooth muscle myosin in the laser trap," (in eng), *J Muscle Res Cell Motil,* vol. 19, no. 8, pp. 825-37, Nov 1998, doi: 10.1023/a:1005489501357.

[26] U. Malmqvist and A. Arner, "Correlation between isoform composition of the 17 kDa myosin light chain and maximal shortening velocity in smooth muscle," (in eng), *Pflugers Arch,* vol. 418, no. 6, pp. 523-30, Jul 1991, doi: 10.1007/bf00370566.

[27] R. A. Murphy, "Contractile system function in mammalian smooth muscle," (in eng), *Blood Vessels,* vol. 13, no. 1-2, pp. 1-23, 1976, doi: 10.1159/000158076.

[28] T. J. Eddinger and R. A. Murphy, "Two smooth muscle myosin heavy chains differ in their light meromyosin fragment," (in eng), *Biochemistry,* vol. 27, no. 10, pp. 3807-11, May 17 1988, doi: 10.1021/bi00410a043.

[29] T. J. Eddinger and D. P. Meer, "Myosin II isoforms in smooth muscle: heterogeneity and function," (in eng), *Am J Physiol Cell Physiol,* vol. 293, no. 2, pp. C493-508, Aug 2007, doi: 10.1152/ajpcell.00131.2007.

[30] A. Sobieszek and J. V. Small, "Regulation of the actin-myosin interaction in vertebrate smooth muscle: activation via a myosin light-chain kinase and the effect of tropomyosin," (in eng), *J Mol Biol,* vol. 112, no. 4, pp. 559-76, Jun 5 1977, doi: 10.1016/s0022-2836(77)80164-2.

[31] R. Léguillette, N. B. Zitouni, K. Govindaraju, L. M. Fong, and A. M. Lauzon, "Affinity for MgADP and force of unbinding from actin of myosin purified from tonic and phasic smooth muscle," (in eng), *Am J Physiol Cell Physiol,* vol. 295, no. 3, pp. C653-60, Sep 2008, doi: 10.1152/ajpcell.00100.2008.

[32] K. M. Trybus and S. Lowey, "Conformational states of smooth muscle myosin. Effects of light chain phosphorylation and ionic strength," (in eng), *J Biol Chem,* vol. 259, no. 13, pp. 8564-71, Jul 10 1984.

[33] W. T. Perrie, L. B. Smillie, and S. B. Perry, "A phosphorylated light-chain component of myosin from skeletal muscle," (in eng), *Biochem J,* vol. 135, no. 1, pp. 151-64, Sep 1973, doi: 10.1042/bj1350151.

[34] M. J. Greenberg, T. R. Mealy, J. D. Watt, M. Jones, D. Szczesna-Cordary, and J. R. Moore, "The molecular effects of skeletal muscle myosin regulatory light chain phosphorylation," *American Journal of Physiology-Regulatory, Integrative and Comparative Physiology,* vol. 297, no. 2, pp. R265-R274, 2009, doi: 10.1152/ajpregu.00171.2009.

[35] H. L. Sweeney and J. T. Stull, "Alteration of cross-bridge kinetics by myosin light chain phosphorylation in rabbit skeletal muscle: implications for regulation of actin-myosin interaction," (in eng), *Proc Natl Acad Sci U S A,* vol. 87, no. 1, pp. 414-8, Jan 1990, doi: 10.1073/pnas.87.1.414.

[36] D. Szczesna, J. Zhao, M. Jones, G. Zhi, J. Stull, and J. D. Potter, "Phosphorylation of the regulatory light chains of myosin affects Ca2+ sensitivity of skeletal muscle contraction," (in eng), *J Appl Physiol (1985),* vol. 92, no. 4, pp. 1661-70, Apr 2002, doi: 10.1152/japplphysiol.00858.2001.

[37] S. Lowey, G. S. Waller, and K. M. Trybus, "Skeletal muscle myosin light chains are essential for physiological speeds of shortening," (in eng), *Nature,* vol. 365, no. 6445, pp. 454-6, Sep 30 1993, doi: 10.1038/365454a0.

[38] P. VanBuren, G. S. Waller, D. E. Harris, K. M. Trybus, D. M. Warshaw, and S. Lowey, "The essential light chain is required for full force production by skeletal muscle myosin," (in eng), *Proc Natl Acad Sci U S A,* vol. 91, no. 26, pp. 12403-7, Dec 20 1994, doi: 10.1073/pnas.91.26.12403.

[39] S. Lowey and K. M. Trybus, "Role of skeletal and smooth muscle myosin light chains," (in eng), *Biophys J,* vol. 68, no. 4 Suppl, pp. 120S-126S; discussion 126S-127S, Apr 1995.

[40] J. Hanson, J. Lowy, M. K. Reedy, A. F. Huxley, and H. E. Huxley, "The structure of actin filaments and the origin of the axial periodicity in the I-substance of vertebrate striated

muscle," *Proceedings of the Royal Society of London. Series B. Biological Sciences,* vol. 160, no. 981, pp. 449-460, 1964, doi: doi:10.1098/rspb.1964.0055.

[41] S. B. Marston and C. W. Smith, "The thin filaments of smooth muscles," (in eng), *J Muscle Res Cell Motil,* vol. 6, no. 6, pp. 669-708, Dec 1985, doi: 10.1007/bf00712237.

[42] K. G. Morgan and S. S. Gangopadhyay, "Invited review: cross-bridge regulation by thin filament-associated proteins," (in eng), *J Appl Physiol (1985),* vol. 91, no. 2, pp. 953-62, Aug 2001, doi: 10.1152/jappl.2001.91.2.953.

[43] J. R. Sellers and M. D. Pato, "The binding of smooth muscle myosin light chain kinase and phosphatases to actin and myosin," (in eng), *J Biol Chem,* vol. 259, no. 12, pp. 7740-6, Jun 25 1984.

[44] L. Smith, X. Su, P. Lin, G. Zhi, and J. T. Stull, "Identification of a novel actin binding motif in smooth muscle myosin light chain kinase," (in eng), *J Biol Chem,* vol. 274, no. 41, pp. 29433-8, Oct 8 1999, doi: 10.1074/jbc.274.41.29433.

[45] R. A. Milligan, M. Whittaker, and D. Safer, "Molecular structure of F-actin and location of surface binding sites," (in eng), *Nature,* vol. 348, no. 6298, pp. 217-21, Nov 15 1990, doi: 10.1038/348217a0.

[46] A. L. Wells *et al.*, "Myosin VI is an actin-based motor that moves backwards," *Nature,* vol. 401, no. 6752, pp. 505-508, 1999/09/01 1999, doi: 10.1038/46835.

[47] I. M. Herman, "Actin isoforms," (in eng), *Curr Opin Cell Biol,* vol. 5, no. 1, pp. 48-55, Feb 1993, doi: 10.1016/s0955-0674(05)80007-9.

[48] D. E. Harris and D. M. Warshaw, "Smooth and skeletal muscle actin are mechanically indistinguishable in the in vitro motility assay," (in eng), *Circ Res,* vol. 72, no. 1, pp. 219-24, Jan 1993, doi: 10.1161/01.res.72.1.219.

[49] G. N. Phillips, Jr., J. P. Fillers, and C. Cohen, "Tropomyosin crystal structure and muscle regulation," (in eng), *J Mol Biol,* vol. 192, no. 1, pp. 111-31, Nov 5 1986, doi: 10.1016/0022-2836(86)90468-7.

[50] S. S. Lehrer, "The regulatory switch of the muscle thin filament: Ca2+ or myosin heads?," (in eng), *J Muscle Res Cell Motil,* vol. 15, no. 3, pp. 232-6, Jun 1994, doi: 10.1007/bf00123476.

[51] H. G. Zot and J. D. Potter, "A structural role for the Ca2+-Mg2+ sites on troponin C in the regulation of muscle contraction. Preparation and properties of troponin C depleted myofibrils," (in eng), *J Biol Chem,* vol. 257, no. 13, pp. 7678-83, Jul 10 1982.

[52] P. Graceffa, "Movement of smooth muscle tropomyosin by myosin heads," *Biochemistry,* vol. 38, no. 37, pp. 11984-11992, 1999/09/01 1999, doi: 10.1021/bi9825495.

[53] P. K. Ngai and M. P. Walsh, "Inhibition of smooth muscle actin-activated myosin Mg2+-ATPase activity by caldesmon," (in eng), *J Biol Chem,* vol. 259, no. 22, pp. 13656-9, Nov 25 1984.

[54] K. Y. Horiuchi and S. Chacko, "Effect of unphosphorylated smooth muscle myosin on caldesmon-mediated regulation of actin filament velocity," (in eng), *J Muscle Res Cell Motil,* vol. 16, no. 1, pp. 11-9, Feb 1995, doi: 10.1007/bf00125306.

[55] T. Okagaki, S. Higashi-Fujime, R. Ishikawa, H. Takano-Ohmuro, and K. Kohama, "In vitro movement of actin filaments on gizzard smooth muscle myosin: requirement of phosphorylation of myosin light chain and effects of tropomyosin and caldesmon," (in eng), *J Biochem,* vol. 109, no. 6, pp. 858-66, Jun 1991, doi: 10.1093/oxfordjournals.jbchem.a123471.

[56] V. P. Shirinsky, K. G. Biryukov, J. M. Hettasch, and J. R. Sellers, "Inhibition of the relative movement of actin and myosin by caldesmon and calponin," (in eng), *J Biol Chem,* vol. 267, no. 22, pp. 15886-92, Aug 5 1992.

[57] I. D. Fraser and S. B. Marston, "In vitro motility analysis of smooth muscle caldesmon control of actin-tropomyosin filament movement," (in eng), *J Biol Chem,* vol. 270, no. 34, pp. 19688-93, Aug 25 1995, doi: 10.1074/jbc.270.34.19688.

[58] K. Y. Horiuchi, H. Miyata, and S. Chacko, "Modulation of smooth muscle actomyosin ATPase by thin filament associated proteins," (in eng), *Biochem Biophys Res Commun,* vol. 136, no. 3, pp. 962-8, May 14 1986, doi: 10.1016/0006-291x(86)90426-2.

[59] H. N. Roman, N. B. Zitouni, L. Kachmar, A. Benedetti, A. Sobieszek, and A. M. Lauzon, "The role of caldesmon and its phosphorylation by ERK on the binding force of unphosphorylated myosin to actin," (in eng), *Biochim Biophys Acta,* vol. 1840, no. 11, pp. 3218-25, Nov 2014, doi: 10.1016/j.bbagen.2014.07.024.

[60] J. R. Haeberle, D. R. Hathaway, and C. L. Smith, "Caldesmon content of mammalian smooth muscles," (in eng), *J Muscle Res Cell Motil,* vol. 13, no. 1, pp. 81-9, Feb 1992, doi: 10.1007/bf01738431.

[61] S. J. Winder, C. Sutherland, and M. P. Walsh, "A comparison of the effects of calponin on smooth and skeletal muscle actomyosin systems in the presence and absence of caldesmon," (in eng), *Biochem J,* vol. 288 (Pt 3), no. Pt 3, pp. 733-9, Dec 15 1992, doi: 10.1042/bj2880733.

[62] S. J. Winder and M. P. Walsh, "Smooth muscle calponin. Inhibition of actomyosin MgATPase and regulation by phosphorylation," (in eng), *J Biol Chem,* vol. 265, no. 17, pp. 10148-55, Jun 15 1990.

[63] J. R. Haeberle, "Calponin decreases the rate of cross-bridge cycling and increases maximum force production by smooth muscle myosin in an in vitro motility assay," (in eng), *J Biol Chem,* vol. 269, no. 17, pp. 12424-31, Apr 29 1994.

[64] H. N. Roman *et al.*, "Unphosphorylated calponin enhances the binding force of unphosphorylated myosin to actin," (in eng), *Biochim Biophys Acta,* vol. 1830, no. 10, pp. 4634-41, Oct 2013, doi: 10.1016/j.bbagen.2013.05.042.

[65] R. Makuch, K. Birukov, V. Shirinsky, and R. Dabrowska, "Functional interrelationship between calponin and caldesmon," (in eng), *Biochem J,* vol. 280 (Pt 1), no. Pt 1, pp. 33-8, Nov 15 1991, doi: 10.1042/bj2800033.

[66] R. A. Murphy, J. T. Herlihy, and J. Megerman, "Force-generating capacity and contractile protein content of arterial smooth muscle," (in eng), *J Gen Physiol,* vol. 64, no. 6, pp. 691-705, Dec 1974, doi: 10.1085/jgp.64.6.691.

[67] W. H. Guilford, D. E. Dupuis, G. Kennedy, J. Wu, J. B. Patlak, and D. M. Warshaw, "Smooth muscle and skeletal muscle myosins produce similar unitary forces and displacements in the laser trap," (in eng), *Biophys J,* vol. 72, no. 3, pp. 1006-21, Mar 1997, doi: 10.1016/s0006-3495(97)78753-8.

[68] R. J. Paul, E. Glück, and J. C. Rüegg, "Cross bridge ATP utilization in arterial smooth muscle," (in eng), *Pflugers Arch,* vol. 361, no. 3, pp. 297-9, Feb 24 1976, doi: 10.1007/bf00587295.

[69] F. S. Fay, D. D. Rees, and D. M. Warshaw, "The contractile mechanism in smooth muscle," in *Membrane Structure and Function*, vol. 4, E. E. Bittar Ed. New York: Wiley and Sons, 1981, pp. 80-130.

[70] D. M. Warshaw, J. M. Desrosiers, S. S. Work, and K. M. Trybus, "Smooth muscle myosin cross-bridge interactions modulate actin filament sliding velocity in vitro," (in eng), *J Cell Biol,* vol. 111, no. 2, pp. 453-63, Aug 1990, doi: 10.1083/jcb.111.2.453.

[71] P. F. Dillon, M. O. Aksoy, S. P. Driska, and R. A. Murphy, "Myosin phosphorylation and the cross-bridge cycle in arterial smooth muscle," (in eng), *Science,* vol. 211, no. 4481, pp. 495-7, Jan 30 1981, doi: 10.1126/science.6893872.

[72] C. M. Hai and R. A. Murphy, "Cross-bridge phosphorylation and regulation of latch state in smooth muscle," (in eng), *Am J Physiol,* vol. 254, no. 1 Pt 1, pp. C99-106, Jan 1988, doi: 10.1152/ajpcell.1988.254.1.C99.

[73] C. M. Hai and R. A. Murphy, "Regulation of shortening velocity by cross-bridge phosphorylation in smooth muscle," (in eng), *Am J Physiol,* vol. 255, no. 1 Pt 1, pp. C86-94, Jul 1988, doi: 10.1152/ajpcell.1988.255.1.C86.

[74] A. Fuglsang, A. Khromov, K. Török, A. V. Somlyo, and A. P. Somlyo, "Flash photolysis studies of relaxation and cross-bridge detachment: higher sensitivity of tonic than phasic smooth muscle to MgADP," (in eng), *J Muscle Res Cell Motil,* vol. 14, no. 6, pp. 666-77, Dec 1993, doi: 10.1007/bf00141563.

[75] A. Khromov, A. V. Somlyo, D. R. Trentham, B. Zimmermann, and A. P. Somlyo, "The role of MgADP in force maintenance by dephosphorylated cross-bridges in smooth muscle: a flash photolysis study," (in eng), *Biophys J,* vol. 69, no. 6, pp. 2611-22, Dec 1995, doi: 10.1016/s0006-3495(95)80132-3.

[76] A. S. Khromov, M. R. Webb, M. A. Ferenczi, D. R. Trentham, A. P. Somlyo, and A. V. Somlyo, "Myosin regulatory light chain phosphorylation and strain modulate adenosine diphosphate release from smooth muscle myosin," (in eng), *Biophys J,* vol. 86, no. 4, pp. 2318-28, Apr 2004, doi: 10.1016/s0006-3495(04)74289-7.

[77] B. Himpens, G. Matthijs, A. V. Somlyo, T. M. Butler, and A. P. Somlyo, "Cytoplasmic free calcium, myosin light chain phosphorylation, and force in phasic and tonic smooth muscle," (in eng), *J Gen Physiol,* vol. 92, no. 6, pp. 713-29, Dec 1988, doi: 10.1085/jgp.92.6.713.

[78] C. Veigel, J. E. Molloy, S. Schmitz, and J. Kendrick-Jones, "Load-dependent kinetics of force production by smooth muscle myosin measured with optical tweezers," (in eng), *Nat Cell Biol,* vol. 5, no. 11, pp. 980-6, Nov 2003, doi: 10.1038/ncb1060.

[79] O. Ogut, S. L. Yuen, and F. V. Brozovich, "Regulation of the smooth muscle contractile phenotype by nonmuscle myosin," (in eng), *J Muscle Res Cell Motil,* vol. 28, no. 7-8, pp. 409-14, 2007, doi: 10.1007/s10974-008-9132-2.

[80] H. Tanaka, K. Homma, H. D. White, T. Yanagida, and M. Ikebe, "Smooth muscle myosin phosphorylated at single head shows sustained mechanical activity," (in eng), *J Biol Chem,* vol. 283, no. 23, pp. 15611-8, Jun 6 2008, doi: 10.1074/jbc.M710597200.

[81] M. J. Siegman, T. M. Butler, and S. U. Mooers, "Energetics and regulation of crossbridge states in mammalian smooth muscle," (in eng), *Experientia,* vol. 41, no. 8, pp. 1020-5, Aug 15 1985, doi: 10.1007/bf01952125.

[82] A. V. Somlyo, Y. E. Goldman, T. Fujimori, M. Bond, D. R. Trentham, and A. P. Somlyo, "Cross-bridge kinetics, cooperativity, and negatively strained cross-bridges in vertebrate smooth muscle. A laser-flash photolysis study," (in eng), *J Gen Physiol,* vol. 91, no. 2, pp. 165-92, Feb 1988, doi: 10.1085/jgp.91.2.165.

[83] T. B. Vyas, S. U. Mooers, S. R. Narayan, J. C. Witherell, M. J. Siegman, and T. M. Butler, "Cooperative activation of myosin by light chain phosphorylation in permeabilized smooth muscle," (in eng), *Am J Physiol,* vol. 263, no. 1 Pt 1, pp. C210-9, Jul 1992, doi: 10.1152/ajpcell.1992.263.1.C210.

[84] S. B. Marston, "What is latch? New ideas about tonic contraction in smooth muscle," (in eng), *J Muscle Res Cell Motil,* vol. 10, no. 2, pp. 97-100, Apr 1989, doi: 10.1007/bf01739965.

[85] P. T. Szymanski, "Calponin (CaP) as a latch-bridge protein--a new concept in regulation of contractility in smooth muscles," (in eng), *J Muscle Res Cell Motil,* vol. 25, no. 1, pp. 7-19, 2004, doi: 10.1023/b:jure.0000021349.47697.bf.

[86] C. Sutherland and M. P. Walsh, "Phosphorylation of caldesmon prevents its interaction with smooth muscle myosin," (in eng), *J Biol Chem,* vol. 264, no. 1, pp. 578-83, Jan 5 1989.

[87] J. Lowy, B. M. Millman, and J. Hanson, "Structure and function in smooth tonic muscles of lamellibranch molluscs," (in eng), *Proc R Soc Lond B Biol Sci,* vol. 160, pp. 525-36, Oct 27 1964, doi: 10.1098/rspb.1964.0068.

[88] T. M. Butler and M. J. Siegman, "Mechanism of catch force: tethering of thick and thin filaments by twitchin," (in eng), *J Biomed Biotechnol,* vol. 2010, p. 725207, 2010, doi: 10.1155/2010/725207.

[89] O. S. Matusovsky, U. V. Shevchenko, G. G. Matusovskaya, A. Sobieszek, A. V. Dobrzhanskaya, and N. S. Shelud'ko, "Catch muscle myorod modulates ATPase activity of Myosin in a phosphorylation-dependent way," (in eng), *PLoS One,* vol. 10, no. 4, p. e0125379, 2015, doi: 10.1371/journal.pone.0125379.

[90] I. G. Vyatchin, U. V. Shevchenko, and N. S. Shelud'ko, "Protein composition of thick filaments from molluscan catch muscle and the role of twitchin in the catch-state formation," (in eng), *Biochem Biophys Res Commun,* vol. 520, no. 3, pp. 634-639, Dec 10 2019, doi: 10.1016/j.bbrc.2019.10.029.

[91] M. P. Sheetz and J. A. Spudich, "Movement of myosin-coated fluorescent beads on actin cables in vitro," (in eng), *Nature,* vol. 303, no. 5912, pp. 31-5, May 5-11 1983, doi: 10.1038/303031a0.

[92] J. A. Spudich, S. J. Kron, and M. P. Sheetz, "Movement of myosin-coated beads on oriented filaments reconstituted from purified actin," (in eng), *Nature,* vol. 315, no. 6020, pp. 584-6, Jun 13-19 1985, doi: 10.1038/315584a0.

[93] T. Yanagida, M. Nakase, K. Nishiyama, and F. Oosawa, "Direct observation of motion of single F-actin filaments in the presence of myosin," (in eng), *Nature,* vol. 307, no. 5946, pp. 58-60, Jan 5-11 1984, doi: 10.1038/307058a0.

[94] S. J. Kron and J. A. Spudich, "Fluorescent actin filaments move on myosin fixed to a glass surface," (in eng), *Proc Natl Acad Sci U S A,* vol. 83, no. 17, pp. 6272-6, Sep 1986, doi: 10.1073/pnas.83.17.6272.

[95] Y. Y. Toyoshima, S. J. Kron, E. M. McNally, K. R. Niebling, C. Toyoshima, and J. A. Spudich, "Myosin subfragment-1 is sufficient to move actin filaments in vitro," (in eng), *Nature,* vol. 328, no. 6130, pp. 536-9, Aug 6-12 1987, doi: 10.1038/328536a0.

[96] C. Toepfer and J. R. Sellers, "Use of fluorescent techniques to study the in vitro movement of myosins," (in eng), *Exp Suppl,* vol. 105, pp. 193-210, 2014, doi: 10.1007/978-3-0348-0856-9_9.

[97] M. A. Rahman, A. Salhotra, and A. Månsson, "Comparative analysis of widely used methods to remove nonfunctional myosin heads for the in vitro motility assay," (in eng), *J Muscle Res Cell Motil,* vol. 39, no. 5-6, pp. 175-187, Dec 2018, doi: 10.1007/s10974-019-09505-1.

[98] H. N. Roman, D. Juncker, and A. M. Lauzon, "A microfluidic chamber to study the dynamics of muscle-contraction-specific molecular interactions," (in eng), *Anal Chem,* vol. 87, no. 5, pp. 2582-7, Mar 3 2015, doi: 10.1021/ac503963r.

[99] S. J. Kron, Y. Y. Toyoshima, T. Q. Uyeda, and J. A. Spudich, "Assays for actin sliding movement over myosin-coated surfaces," (in eng), *Methods Enzymol,* vol. 196, pp. 399-416, 1991, doi: 10.1016/0076-6879(91)96035-p.

[100] G. Ijpma, Z. Balassy, and A.-M. Lauzon, "Rapid time-stamped analysis of filament motility," *Journal of Muscle Research and Cell Motility,* vol. 39, no. 5, pp. 153-162, 2018/12/01 2018, doi: 10.1007/s10974-019-09503-3.

[101] S. S. Work and D. M. Warshaw, "Computer-assisted tracking of actin filament motility," (in eng), *Anal Biochem,* vol. 202, no. 2, pp. 275-85, May 1 1992, doi: 10.1016/0003-2697(92)90106-h.

[102] S. Umemoto and J. R. Sellers, "Characterization of in vitro motility assays using smooth muscle and cytoplasmic myosins," (in eng), *J Biol Chem,* vol. 265, no. 25, pp. 14864-9, Sep 5 1990.

[103] L. Hilbert, Z. Balassy, N. B. Zitouni, M. C. Mackey, and A. M. Lauzon, "Phosphate and ADP differently inhibit coordinated smooth muscle myosin groups," (in eng), *Biophys J,* vol. 108, no. 3, pp. 622-31, Feb 3 2015, doi: 10.1016/j.bpj.2014.12.008.

[104] D. M. Warshaw, J. M. Desrosiers, S. S. Work, and K. M. Trybus, "Effects of MgATP, MgADP, and Pi on actin movement by smooth muscle myosin," (in eng), *J Biol Chem,* vol. 266, no. 36, pp. 24339-43, Dec 25 1991.

[105] D. E. Harris, S. S. Work, R. K. Wright, N. R. Alpert, and D. M. Warshaw, "Smooth, cardiac and skeletal muscle myosin force and motion generation assessed by cross-bridge mechanical interactions in vitro," (in eng), *J Muscle Res Cell Motil,* vol. 15, no. 1, pp. 11-9, Feb 1994, doi: 10.1007/bf00123828.

[106] D. Warshaw and K. Trybus, "In vitro evidence for smooth muscle crossbridge mechanical interactions," (in eng), *Adv Exp Med Biol,* vol. 304, pp. 53-9, 1991, doi: 10.1007/978-1-4684-6003-2_6.

[107] A. Ashkin, "Acceleration and trapping of particles by radiation pressure," *Physical Review Letters,* vol. 24, no. 4, pp. 156-159, 01/26/ 1970, doi: 10.1103/PhysRevLett.24.156.

[108] S. Chu, J. E. Bjorkholm, A. Ashkin, and A. Cable, "Experimental observation of optically trapped atoms," (in eng), *Phys Rev Lett,* vol. 57, no. 3, pp. 314-317, Jul 21 1986, doi: 10.1103/PhysRevLett.57.314.

[109] A. Ashkin and J. M. Dziedzic, "Optical trapping and manipulation of viruses and bacteria," (in eng), *Science,* vol. 235, no. 4795, pp. 1517-20, Mar 20 1987, doi: 10.1126/science.3547653.

[110] A. Ashkin, J. M. Dziedzic, and T. Yamane, "Optical trapping and manipulation of single cells using infrared laser beams," *Nature,* vol. 330, no. 6150, pp. 769-771, 1987/12/01 1987, doi: 10.1038/330769a0.

[111] M. W. Berns, W. H. Wright, B. J. Tromberg, G. A. Profeta, J. J. Andrews, and R. J. Walter, "Use of a laser-induced optical force trap to study chromosome movement on the mitotic spindle," *Proceedings of the National Academy of Sciences,* vol. 86, no. 12, pp. 4539-4543, 1989, doi: 10.1073/pnas.86.12.4539.

[112] S. M. Block, D. F. Blair, and H. C. Berg, "Compliance of bacterial flagella measured with optical tweezers," *Nature,* vol. 338, no. 6215, pp. 514-518, 1989/04/01 1989, doi: 10.1038/338514a0.

[113] NobelPrize.org. "Press Release: The Nobel Prize in Physics 2018." Nobel Prize Outreach AB. https://www.nobelprize.org/prizes/physics/2018/press-release/ (accessed July 26, 2021).

[114] R. M. Simmons, J. T. Finer, S. Chu, and J. A. Spudich, "Quantitative measurements of force and displacement using an optical trap," (in eng), *Biophys J,* vol. 70, no. 4, pp. 1813-22, Apr 1996, doi: 10.1016/s0006-3495(96)79746-1.

[115] A. Ashkin, "Forces of a single-beam gradient laser trap on a dielectric sphere in the ray optics regime," *Biophysical Journal,* vol. 61, no. 2, pp. 569-582, 1992/02/01/ 1992, doi: https://doi.org/10.1016/S0006-3495(92)81860-X.

[116] A. Ashkin, "Optical trapping and manipulation of neutral particles using lasers," *Proceedings of the National Academy of Sciences,* vol. 94, no. 10, pp. 4853-4860, 1997, doi: 10.1073/pnas.94.10.4853.

[117] M. Sarshar, W. T. Wong, and B. Anvari, "Comparative study of methods to calibrate the stiffness of a single-beam gradient-force optical tweezers over various laser trapping powers," (in eng), *J Biomed Opt,* vol. 19, no. 11, p. 115001, 2014, doi: 10.1117/1.Jbo.19.11.115001.

[118] S. M. Block, L. S. B. Goldstein, and B. J. Schnapp, "Bead movement by single kinesin molecules studied with optical tweezers," *Nature,* vol. 348, no. 6299, pp. 348-352, 1990/11/01 1990, doi: 10.1038/348348a0.

[119] S. C. Kuo and M. P. Sheetz, "Force of single kinesin molecules measured with optical tweezers," (in eng), *Science,* vol. 260, no. 5105, pp. 232-4, Apr 9 1993, doi: 10.1126/science.8469975.

[120] K. Svoboda, C. F. Schmidt, B. J. Schnapp, and S. M. Block, "Direct observation of kinesin stepping by optical trapping interferometry," *Nature,* vol. 365, no. 6448, pp. 721-727, 1993/10/01 1993, doi: 10.1038/365721a0.

[121] H. Miyata *et al.*, "Stepwise motion of an actin filament over a small number of heavy meromyosin molecules is revealed in an in vitro motility assay," *The Journal of Biochemistry,* vol. 115, no. 4, pp. 644-647, 1994, doi: 10.1093/oxfordjournals.jbchem.a124389.

[122] J. T. Finer, R. M. Simmons, and J. A. Spudich, "Single myosin molecule mechanics: piconewton forces and nanometre steps," (in eng), *Nature,* vol. 368, no. 6467, pp. 113-9, Mar 10 1994, doi: 10.1038/368113a0.

[123] M. J. Tyska *et al.*, "Two heads of myosin are better than one for generating force and motion," (in eng), *Proc Natl Acad Sci U S A,* vol. 96, no. 8, pp. 4402-7, Apr 13 1999, doi: 10.1073/pnas.96.8.4402.

[124] J. E. Molloy, J. E. Burns, J. Kendrick-Jones, R. T. Tregear, and D. C. S. White, "Movement and force produced by a single myosin head," *Nature,* vol. 378, no. 6553, pp. 209-212, 1995/11/01 1995, doi: 10.1038/378209a0.

[125] Z. Balassy, "Can we reproduce the latch-state in vitro at the molecular level?," Master of Engineering in Biological and Biomedical Engineering, Department of Biomedical Engineering, McGill University, Montreal, Canada, 2018.

[126] A. Sobieszek, "Smooth muscle myosin: molecule conformation, filament assembly and associated regulatory enzymes," 1994, pp. 1-29.

[127] A. Sobieszek, J. Borkowski, and V. S. Babiychuk, "Purification and characterization of a smooth muscle myosin light chain kinase-phosphatase complex," (in eng), *J Biol Chem,* vol. 272, no. 11, pp. 7034-41, Mar 14 1997, doi: 10.1074/jbc.272.11.7034.

[128] A. Sobieszek, E. B. Babiychuk, B. Ortner, and J. Borkowski, "Purification and characterization of a kinase-associated, myofibrillar smooth muscle myosin light chain phosphatase possessing a calmodulin-targeting subunit," (in eng), *J Biol Chem,* vol. 272, no. 11, pp. 7027-33, Mar 14 1997, doi: 10.1074/jbc.272.11.7027.

[129] N. Suzuki, H. Miyata, S. Ishiwata, and K. Kinosita, Jr., "Preparation of bead-tailed actin filaments: estimation of the torque produced by the sliding force in an in vitro motility assay," (in eng), *Biophys J,* vol. 70, no. 1, pp. 401-8, Jan 1996, doi: 10.1016/s0006-3495(96)79583-8.

[130] D. E. Dupuis, W. H. Guilford, J. Wu, and D. M. Warshaw, "Actin filament mechanics in the laser trap," (in eng), *J Muscle Res Cell Motil,* vol. 18, no. 1, pp. 17-30, Feb 1997, doi: 10.1023/a:1018672631256.

[131] T. I. A. f. t. P. o. W. a. Steam, "Release on the IAPWS formulation 2008 for the viscosity of ordinary water substance," Berlin, Germany, 2008. [Online]. Available: http://www.iapws.org/relguide/viscosity.html

[132] L. Merkel, W. T. Gerthoffer, and T. J. Torphy, "Dissociation between myosin phosphorylation and shortening velocity in canine trachea," (in eng), *Am J Physiol,* vol. 258, no. 3 Pt 1, pp. C524-32, Mar 1990, doi: 10.1152/ajpcell.1990.258.3.C524.